JACS Au
AN OPEN ACCESS JOURNAL OF THE AMERICAN CHEMICAL SOCIETY

pubs.acs.org/jacsau

Article

Molecular-Level Control over Ionic Conduction and Ionic Current Direction by Designing Macrocycle-Based Ionomers

Shyambo Chatterjee,[†] Ehsan Zamani,[†] Seefat Farzin,[†] Iman Evazzade, Oghenetega Allen Obewhere, Tyler James Johnson, Vitaly Alexandrov, and Shudipto Konika Dishari*

Cite This: *JACS Au* 2022, 2, 1144−1159

Read Online

ACCESS | Metrics & More | Article Recommendations | Supporting Information

ABSTRACT: Poor ionic conductivity of the catalyst-binding, sub-micrometer-thick ionomer layers in energy conversion and storage devices is a huge challenge. However, ionomers are rarely designed keeping in mind the specific issues associated with nanoconfinement. Here, we designed nature-inspired ionomers (calix-2) having hollow, macrocyclic, calix[4]arene-based repeat units with precise, sub-nanometer diameter. In ≤100 nm-thick films, the in-plane proton conductivity of calix-2 was up to 8 times higher than the current benchmark ionomer Nafion at 85% relative humidity (RH), while it was 1−2 orders of magnitude higher than Nafion at 20−25% RH. Confocal laser scanning microscopy and other synthetic techniques allowed us to demonstrate the role of macrocyclic cavities in boosting the proton conductivity. The systematic self-assembly of calix-2 chains into ellipsoids in thin films was evidenced from atomic force microscopy and grazing incidence small-angle X-ray scattering measurements. Moreover, the likelihood of alignment and stacking of macrocyclic units, the presence of one-dimensional water wires across this macrocycle stacks, and thus the formation of long-range proton conduction pathways were suggested by atomistic simulations. We not only did see an unprecedented improvement in thin-film proton conductivity but also saw an improvement in proton conductivity of bulk membranes when calix-2 was added to the Nafion matrices. Nafion−calix-2 composite membranes also took advantage of the asymmetric charge distribution across calix[4]arene repeat units collectively and exhibited voltage-gating behavior. The inclusion of molecular macrocyclic cavities into the ionomer chemical structure can thus emerge as a promising design concept for highly efficient ion-conducting and ion-permselective materials for sustainable energy applications.

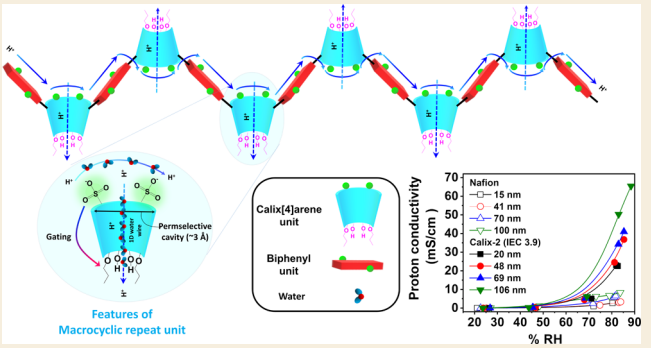

KEYWORDS: *ionomer, porin-inspired, water wire, proton conductivity, gating, ion channel, thin film, fuel cell*

INTRODUCTION

Ionomers with high ionic conductivity and permselectivity are highly needed to address the technical challenges of energy conversion and storage devices (such as fuel cells, electrolyzers, and batteries).[1−4] Ionomers are used as several tens of micrometer-thick, bulk, free-standing membrane separator and a sub-micrometer-thick catalyst binding layer in these devices. However, hydrogen fuel cells experience a major ion transport limitation within the sub-micrometer-thick ionomer layer.[5−8] This slows down the electrocatalytic reaction at the cathode and affects the performance of the device. A ∼25 μm-thick bulk, free-standing membrane of the current state-of-the-art, fluorocarbon-based ionomer Nafion, conducts protons efficiently, while the proton conductivity of the same ionomer becomes about an order of magnitude lower in a ∼25 nm-thick film on the substrate.[6,9,10] The high conductivity in bulk membrane[11−17] and low conductivity in thin films/catalyst layers[5,18−20] have also been reported for polyaromatic ionomers. While there have been significant efforts to design ionomers to improve the ionic conductivity of bulk membranes,[15−17,21,22] ionomers are rarely designed keeping in mind the specific issues associated with nanoscale confined thin films and with a target to improve thin-film ionic conductivity.[23−25]

In sub-micrometer-thick films of conventional ionomers (such as Nafion), the phase segregation and ionic domain connectivity are sacrificed due to dimensional and interfacial constraints.[23,26−31] These cause a decrease in the size of ion-conducting domains to ∼1.5−2 nm in sub-micrometer-thick, hydrated Nafion films[32] from ∼4 nm in corresponding bulk membranes.[33] Based on the current understanding of

Received: March 3, 2022
Revised: April 22, 2022
Accepted: April 28, 2022
Published: May 11, 2022

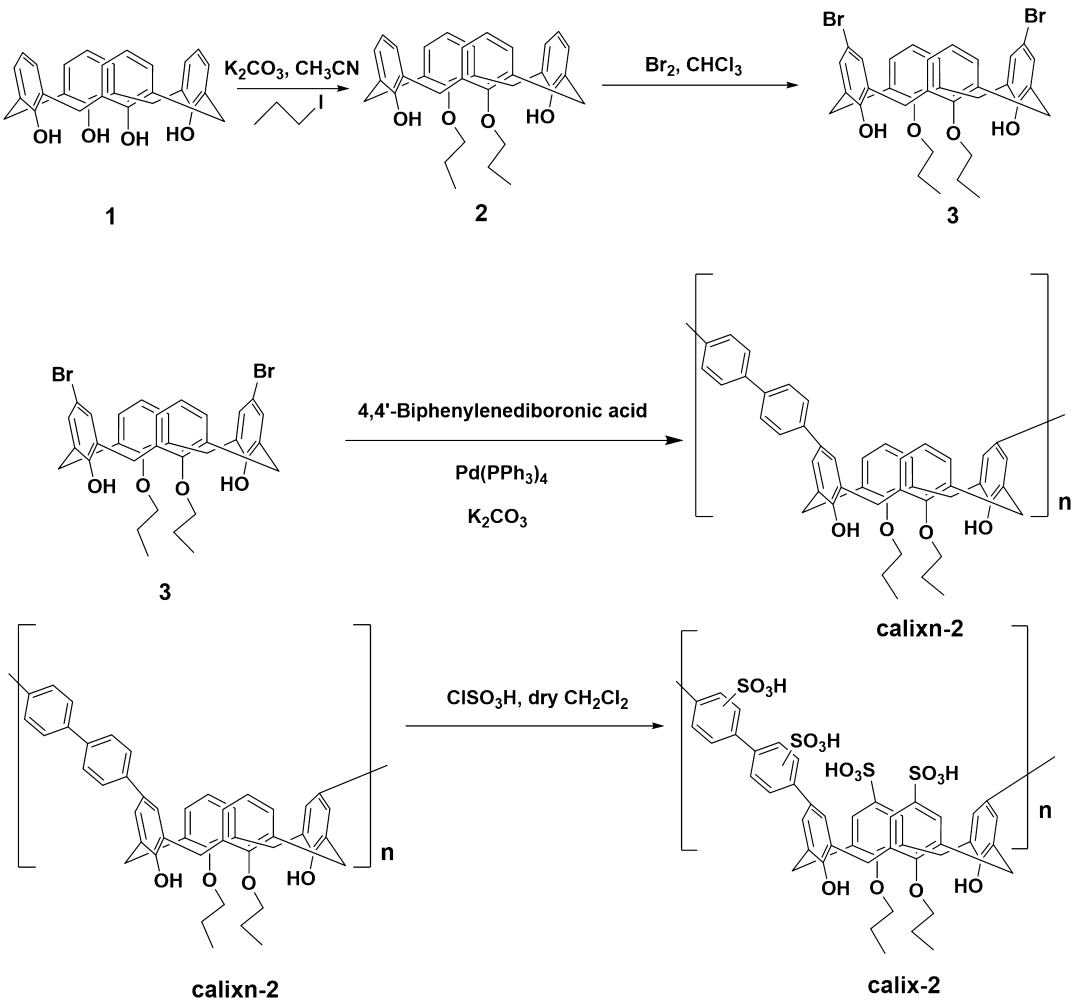

Figure 1. Synthesis procedure of the calixn-2 and calix-2 ionomer.

ionomers, a common school of thought is that ion channels with a narrow diameter (≤2 nm) cause nanoconfinement effects on flow and negatively impact the proton conductivity.[28,32] However, the trends in proton conduction through narrow (1−2 nm) *versus* very narrow (sub-nanometer) ion channels are very thought-provoking.[34] In fact, natural porin-based systems (such as gramicidin A[35]) exhibit an exceptionally high ionic conductivity despite having sub-nanometer-sized ion channels.

Porins self-assemble within biological membranes and are responsible for the controlled transport of water and ions across living cells. The hydrophobic moieties, lined along the inner surface of the porins, enable faster water transport,[36] while the appended functional groups give porins the capability to transport ions selectively.[37−41] Researchers, inspired by these features, have designed synthetic fluid/ion channels[42,43] based on dendritic dipeptides,[44] imidazole I-quartets,[42,45] functionalized calix[46]/pillararenes,[42,43,47−49] carbon nanotubes (CNTs),[34,50−52] graphene oxide,[53] and more.[54−57] These artificial systems have been studied as single transport elements[46,48,49,51] or self-assembled features comprising several monomeric units[46,47] upon embedding within lipid bilayers,[46−48,51,54] polymers,[49,50,52] or inorganic[51,58] matrices. CNTs with narrow diameters allow fluid flow in a frictionless manner,[50] which is best explained by slip flow.[50,55,59] CNTs[34,51] with varying diameters (∼0.8−2 nm) and some pillar[5]arene-derivatives (diameter ∼0.5 nm)[47,56] showed interesting trends in proton conductivity within the narrow constrictions of molecular cavities. Noy *et al.*[34] reported that when the diameter of CNTs was ∼1.5 nm, the proton transport rate was comparable to bulk water. However, when the diameter went below 1 nm (∼0.8 nm), the proton transport rate exceeded that of bulk water and gramicidin-based biological ion channels (diameter ∼0.4 nm). Molecular dynamics simulation of CNTs[60] suggested that inside channels with angstrom-scale diameter, the water molecules form strongly connected, one-dimensional, hydrogen-bonded water wires (1D water wire effect[35,61]), while wider CNTs preserve an almost bulk-like, random water arrangement. Previous work on gramicidin A also supports that reorientational relaxation of water molecules, a prerequisite for proton conduction, is possible along water wires in such narrow channels.[62] Thus, confinement can go in favor of proton conduction, rather than going against if the diameter of the synthetic ion channels is carefully chosen to enable the formation of 1D water wires.

Among the synthetic, porous, solid-state proton conductors, metal−organic frameworks,[63] covalent organic frameworks,[64] and polymers of intrinsic microporosity[65] are the most promising classes. While each of these have unique advantages, the porous material design community is still working to address several challenges and achieve a combination of characteristics, such as precise pores preferably with angstrom-

https://doi.org/10.1021/jacsau.2c00143
JACS Au 2022, 2, 1144−1159

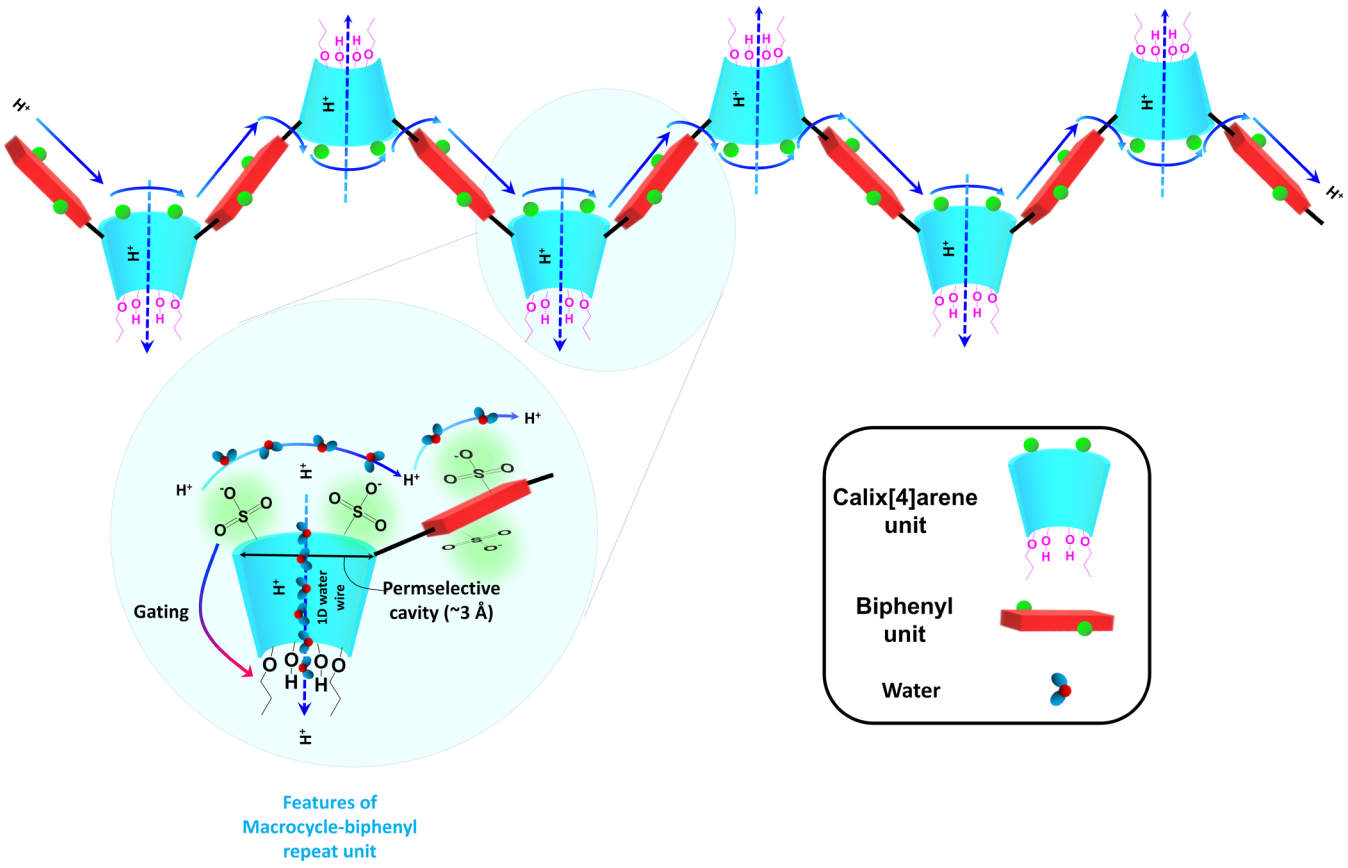

Figure 2. Schematic showing possible proton conduction pathways in calix-2 ionomeric systems: along the chain (solid blue arrows) and across macrocyclic cavities (dotted blue arrows) (top). The unique design features of macrocyclic repeat units of calix-2 ionomers [precise sub-nanometer-sized permselective cavity (3 Å), 1D water wire, gating] (bottom left). The green balls, appended to macrocyclic calix[4]arene and biphenyl units, represent sulfonic acid ($-SO_3H$) groups which participate in the along-chain ion transport.

scale diameter to attain faster ion diffusion with permselectivity,[64,66] narrow pore size distribution,[67] solubilities in conventional organic solvents to enhance processability,[63] good dispersibility and compatibility with matrix materials of catalyst inks,[63] low environmental impacts,[63,67] and scalability.[63] Lastly, but most importantly, we need good ionic conductivity in sub-micrometer-thick films to improve the interfacial ion transport behavior, a critical, but rarely addressed issue of hydrogen fuel cells, electrolyzers, and other electrochemical devices.[23,68]

Considering these needs, here, we report a new class of nature-inspired ionomers (calix-2, Figure 1) having sulfonated macrocyclic calix[4]arene-based repeat units with a target to improve thin-film proton conductivity. Macrocycles or other sub-nanometer precision materials are widely used for ion sensing,[69,70] host−guest interaction studies,[71−74] gas separation,[75,76] and desalination/ion-selective separations.[43,55,77−82] Very limited attempts have incorporated calix[*n*]arenes within inorganic[58,83] ion-transporting membranes, but in the monomeric form. Therefore, the incorporation of macrocyclic repeat units within the chemical structure of oligo/polymers is still a new concept in ionomer design for energy conversion/storage devices.

The calix-2 ionomers, we designed, possess multiple unique features, which can address the aforementioned design challenges of ion-conducting materials currently used. Calix[4]arene has a rigid macrocyclic core with a diameter of ∼3 Å[84] (can vary up to +2 Å depending on the substituting groups[85]). Therefore, calix-2 can leverage the 1D water wire effect and allow faster passage of ions through the sub-nanometer-sized macrocyclic cavities (Figure 2). We hypothesize that the aromatic ionomers having macrocycle-based repeat units along the chain can leverage multiscale ion transport pathways: (i) along the $-SO_3H$ groups of all units (macrocyclic and nonmacrocyclic) of an ionomer chain and (ii) across macrocyclic cavities. Even if the ionomer chains experience severe confinement and fail to spontaneously phase-segregate (as seen in sub-micrometer-thick Nafion films[7,10,26,27]), the individual macrocyclic repeat units of calix-2 chains can still maintain the through-cavity ionic conduction. On top of this, if we are able to achieve favorable self-assembly of pore-forming units in solution (likely based on prior evidences[73,86−91]) and retain the self-assembled feature of the solid-state, we will be able to achieve both short-range and long-range ionic conduction simultaneously. Such features can also be beneficial to improve bulk membrane proton conductivity. These macrocycle-based ionomers are also versatile as their chemical functionalities can be tuned to make them soluble in common organic solvents. They can form smooth, thin films and can be made compatible with the components of catalyst inks, especially hydrocarbon-based catalysts[92,93] that are being designed as low-cost alternatives for fuel cells. Besides the 1D water wire effect, by creating charge distribution asymmetry at the upper and lower rims of the macrocyclic repeat units,[39,41,42,54] we have been able to achieve voltage gating, a unique feature of natural[94,95] and nature-mimicking systems.[54−57] A composite, bulk membrane,

https://doi.org/10.1021/jacsau.2c00143
JACS Au 2022, 2, 1144−1159

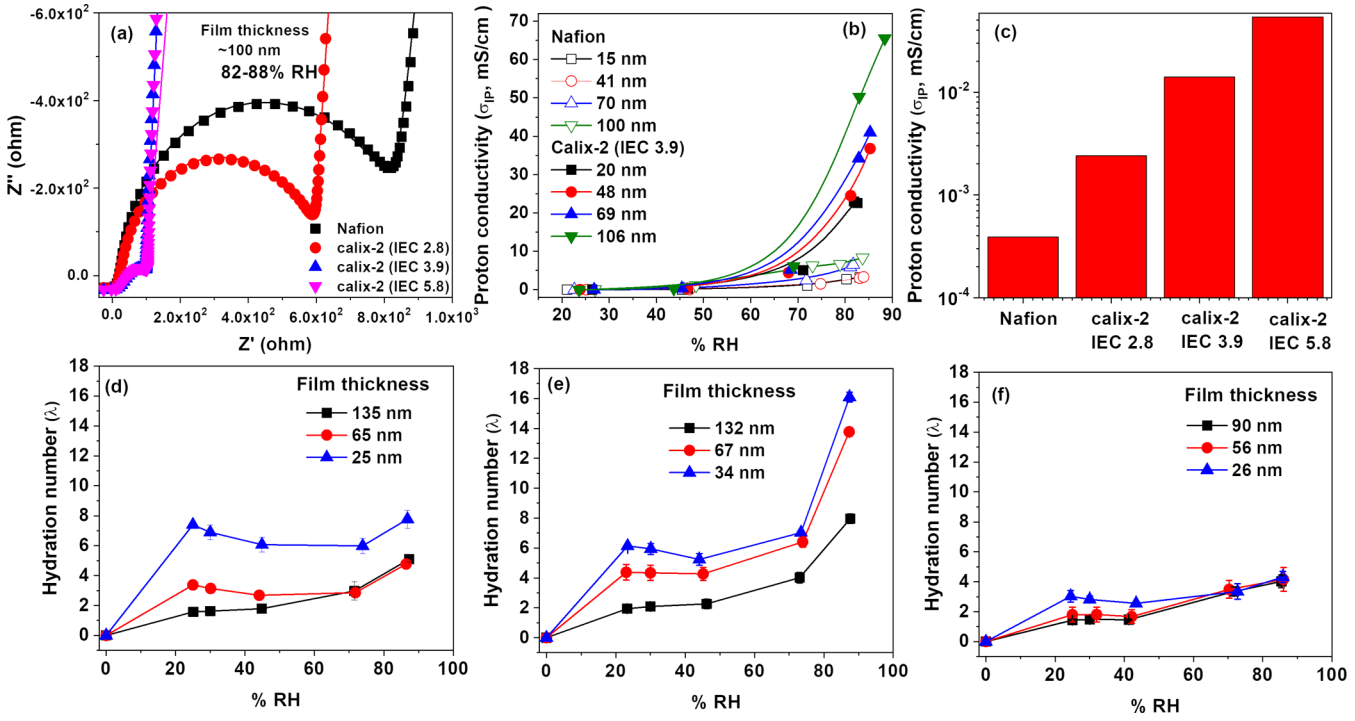

Figure 3. In-plane impedance curves of ~100 nm-thick unannealed Nafion and calix-2 films with different IECs (a); in-plane proton conductivity (σ_{IP}) of Nafion and calix-2 (IEC 3.9) films with different thicknesses as a function of % RH (b); in-plane proton conductivity (σ_{IP}) of Nafion and calix-2 thin films (~15 nm) at 20–25% RH (c). Water uptake [in the form of hydration number (λ)] of sub-micrometer-thick films of calix-2 with IECs 2.8 (d); 3.9 (e) and 5.8 (f) as a function of film thickness and % RH. The λ values were calculated as the moles of water absorbed per mole of sulfonic acid ($-SO_3H$) in the ionomer samples. All measurements were done at room temperature (~23 °C).

containing calix-2 with Nafion, can thus control the direction of ion transport. Such materials have great potential to design permselective membranes for flow batteries and many other electrochemical devices.

RESULTS AND DISCUSSION

Synthesis of Ionomers

Figure 1 shows the synthetic routes to obtain the neutral precursor of the calix[4]arene-based oligomer (calixn-2) and sulfonated ionomer (calix-2). In calix-2, the upper-rim sulfonated calix[4]arene units are present alternating with sulfonated biphenyl-based repeat units along the ionomer backbone. In brief, the dibromo derivative of calix[4]arene (3) was synthesized by alkylation, followed by the bromination reaction [Figures S1–S4, S7, and S8 for NMR and HR-TOF MS spectra of compounds (**2**) and (**3**)]. This dibromo-derivative of calix[4]arene (**3**) was then Suzuki cross-coupled to the boronic acid-functionalized biphenyl monomer to yield neutral calixn-2 (Figures S5 and S6). Similar to compounds (**2**) and (**3**), the ^{1}HNMR spectra for calixn-2 (Figure S5) showed the signal for the methylene bridges (at 3.40 and 4.35 ppm), which indicated that the cone conformation was retained in calixn-2. Calixn-2 was sulfonated further using chlorosulfonic acid ($ClSO_3H$) to obtain calix-2 ionomers. By varying the concentration of $ClSO_3H$ in the reaction system, sulfonated calix-2 with different ion exchange capacities (IECs) (2.8, 3.9, and 5.8) was obtained (please see the Methods section of the paper and the Supporting Information for synthetic details). It is to be noted that 4 was the maximum possible IEC if all the $-SO_3H$ groups in the sample were covalently bonded to the ionomer chains. Since the ionomer was capable of capturing free acids, we explored a version of calix-2 with an IEC higher than 4 (IEC 5.8), where the contribution of acid groups was partially from the covalently bonded $-SO_3H$ groups and the rest was from the free acids trapped within the macrocyclic cavities of calix[4]arene units. Multiple water-wash and ultrasonication cycles ensured the removal of unreacted acids from sulfonated calix-2 samples, as confirmed by the carbon/sulfur (C/S) ratio from XPS [4.52 (experimental) and 4.32 (theoretical)]. Additionally, dialysis for extended hours (72 h) was performed for calix-2 (IEC 5.8) to ensure the removal of excess free/untrapped acids. The low % Cl in IEC 2.8 (0%) and 3.9 (4.16%) samples also supported the satisfactory purification of the compounds, while high % Cl in the IEC 5.8 sample confirmed the trapping of unreacted $ClSO_3H$, which was most likely happening in the macrocyclic cavities of calix[4]arene units of calix-2.

The number-average molecular weights (M_n) of calix-2 samples [5671 (IEC 2.8) and 6138 (IEC 3.9)] were at the lower-molecular-weight end of polymers and can thus be called as oligomers. They can still be considered as ionomers due to their excellent ionic conduction capabilities even in sub-micrometer-thick films (discussed later). Also, thermogravimetric analysis (TGA) showed that calixn-2 was thermally stable until 270 °C (Figure S9). Last but not the least, these ionomers made smooth films (over substrates) within the thickness range (~15–100 nm) comparable to the catalyst-binding ionomer layers over electrodes. Such thin-film processability is critical for making fuel-cell electrodes.[96] The significantly lower density of calix-2 films (as compared to Nafion, Table S1) could be attributed to the porosity induced by macrocyclic cavities of calix[4]arene.

https://doi.org/10.1021/jacsau.2c00143
JACS Au 2022, 2, 1144–1159

Proton Conductivity in Thin Films

Figure 3a−c shows the in-plane proton conduction behavior (σ_{IP}) of calix-2 ionomers in ∼15−100 nm-thick films as a function of IEC, film thickness, and relative humidity (% RH). The in-plane impedance measurements were done using interdigitated electrode arrays deposited on SiO_2 substrates (please see the Supporting Information for further details). The semicircular regions of the impedance curves of ∼100 nm-thick films of Nafion and calix-2 (at three different IECs: 2.8, 3.9, and 5.8) at ∼82−88% RH indicated that the film resistance values of calix-2 films were always lower than that of Nafion (Figure 3a). When the impedance curves were fitted to an equivalent circuit model (Figure S10 for representative data fits), we saw significantly higher proton conductivity of calix-2 films as compared to Nafion films with similar thickness and similar % RH. For example, a ∼100 nm-thick Nafion film showed an in-plane proton conductivity of ∼8.31 mS/cm (Figure 3b), while the calix-2 films showed proton conductivity values of ∼10.80 mS/cm (IEC 2.8), 65.48 mS/cm (IEC 3.9, Figure 3b), and 62.13 mS/cm (IEC 5.8) at ∼85% RH (Table S2). This means that calix-2 can offer proton conductivity up to 8 times higher than that of Nafion under high-humidity conditions in thin films. The proton conductivity values of calix-2 films were also higher than those of Nafion films in the out-of-plane direction (σ_{OP}, Figure S11 and Table S3). Such an improvement in proton conductivity in thin films is unprecedented. The improvement in proton conductivity was even higher under low-humidity conditions. For example, ∼20 nm-thick calix-2 films (IEC 3.9, 5.8) showed conductivity (σ_{IP}) ∼5−8 times higher than that of Nafion at ∼85% RH (Table S2), while the same films showed up to 1−2 orders of magnitude improvement in ionic conductivity at 20−25% RH (Figure 3c). The films we studied had thickness comparable to that of the ionomer-based binder layers over catalyst particles in hydrogen fuel cells and electrolyzers. Especially, such improvement in proton conductivity at low % RH stands out[97] as most of the reported ionomers (both fluorocarbon- and hydrocarbon-based) showed poor proton conductivity at low % RH in both bulk membranes[98−100] and the thin film[7,8,101] format.

The EIS data above and our prior understanding of synthetic ion channels[34,42,54,60,62] suggested that the exceedingly high proton conductivity of calix-2 films originated from the sulfonated macrocyclic cavities. It is a well-known fact that ionic domain or ion channel connectivity and appropriate size of water confinement are critical for proton transport. Bulk-like water, present in ∼4 nm-size ionic domains in thick Nafion membranes,[33,102] makes the proton conductivity facile. On the contrary, in sub-micrometer-thick Nafion films, the interfacial interactions and dimensional restrictions impede the phase segregation.[10] As a result, the confined water molecules form ∼1.5−2.3 nm-sized ionic domains on an average (Figure S12a,b)[28,32] and lead to poor proton conductivity[5,8,10,101,103−105] in thin Nafion films. Macrocyclic cavities can have the capabilities to address and overcome this thin film proton transport barrier. First of all, the hollow cavities can act like ion channels and provide additional ion conduction pathways in thin ionomer films. Moreover, the sub-micrometer-sized constrictions of molecular cavities have certain advantages in transporting ions faster,[34,35] which is not possible to achieve with ∼1−2 nm-sized ionic domains (present in Nafion thin films). Based on the extensive prior studies on structural and orientational dynamics of water, the sub-nanometer-sized cavities can compel water molecules (∼2.8 Å)[36] to align and form a single file of water.[35] If there are no interactive restrictions (*e.g.*, H-bonding or dipole−dipole interactions) inside and across the cavities/channel, water dipoles tend to orient in the same direction and parallel to the cavity axis[36] to create 1D, H-bonded water wires.[60] Rapid proton hopping, facilitated by such highly ordered, defect-free water wires,[35,61] has been identified as one of the key reasons behind very fast proton transport rates in gramicidin A (4 Å)[35] and CNTs with <1 nm diameter.[34] These water wires are superior to bulk water as in bulk water, the order of water dipoles is still random.[61,106] Since calix[4]arene has sub-nanometer-sized macrocyclic cavities (∼3 Å),[84] it is likely that calix-2 also has a similar proton transport phenomenon.

To reveal whether the high proton conductivity of calix-2 was actually caused by calix[4]arene cavities, we performed several experiments. First, we synthesized a nonmacrocycle-containing version of ionomer (sulfonated biphenyl polymer (SBP), Figure S13a,b). While calix-2 had both sulfonated biphenyl and macrocyclic sulfonated calix[4]arene repeat units, SBP only had sulfonated biphenyl repeat units. The non-macrocycle-containing SBP showed very weak in-plane proton conductivity as compared to calix-2 in films with similar thickness. For example, a ∼49 nm-thick SBP film showed a proton conductivity of 7×10^{-4} mS/cm (Figure S13c), while it was 37 mS/cm for the calix-2 film at ∼80−83% RH. In another set of experiments, we showed the effect of the inclusion of macrocycles by making a composite film out of SBP and monomeric sulfonated calix[4]arene (Scalixmono, Figure S13) in a 1:0.2 wt ratio. The (SBP−Scalixmono) composite film (∼47 nm thick) showed a proton conductivity of 17.5 mS/cm (Figure S13d), which was ∼5 orders of magnitude higher than that of the pure SBP film. All these evidences confirmed the role of hollow macrocyclic cavities in achieving exceptional improvement in proton conductivity in thin films.

As can be seen from the chemical structure, the calix-2 ionomers were composed of both sulfonated calix[4]arene and sulfonated biphenyl repeat units along the backbone. Therefore, the ionomers indeed had the capability to facilitate ion transport in two directions: (i) the $-SO_3H$ groups along the main chain and (ii) across the cavity of sulfonated macrocyclic calix[4]arene units. Thus, the relative contribution of along-chain and through-cavity transport on the in-plane and out-of-plane conductivity will be decided by how the chains are packed and how the self-assembled features are oriented[73,86−88] in a film/membrane [discussed in the atomic force microscopy (AFM) and Atomistic Simulation sections later].

Water Uptake

Figure 3d−f shows the water uptake of ∼25−135 nm-thick calix-2 films as a function of % RH, film thickness, and IEC. Increasing the IEC of the ionomers from 2.8 to 3.9 led to an increase in the hydration number (λ), especially at high % RH. This is a common trend of typical ionomers[107] and could be attributed to an increase in the degree of sulfonation of the ionomer. However, increasing the IEC further (to 5.8) caused a decrease in λ values. For example, at ∼85% RH, the λ values of ∼25−30 nm-thick films of calix-2 decreased from ∼16 to ∼4 when the IEC increased from 3.9 to 5.8. It is to be noted that the IEC 5.8-variant of calix-2 had ion-conducting groups both in the form of covalently bonded $-SO_3H$ groups (to aromatic rings) and doped free acids. These free acids are likely to take

https://doi.org/10.1021/jacsau.2c00143
JACS Au 2022, 2, 1144−1159

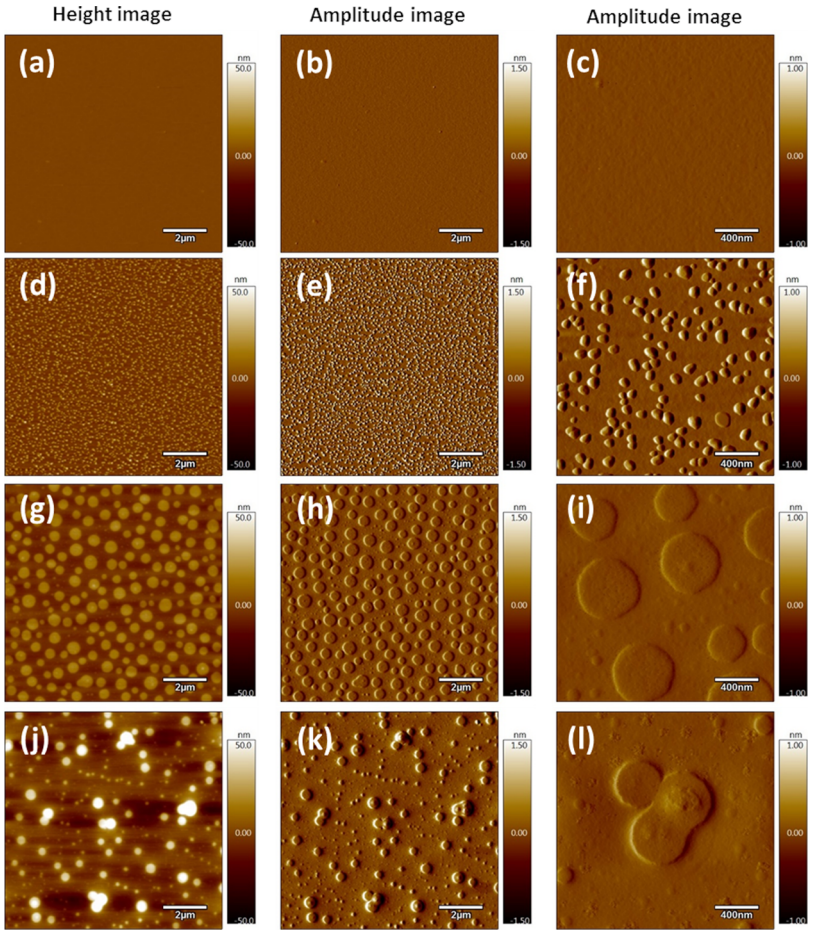

Figure 4. AFM height and amplitude images of ∼35 nm-thick films of Nafion (a–c) and calix-2 with IECs 2.8 (d–f); 3.9 (g–i); and 5.8 (j–l). The scale bars are shown within the images.

place inside the macrocyclic cavities and block them, which could otherwise be taken by water. This may be a reason why IEC 5.8 films could not show proton conductivity higher than IEC 3.9 films at a high % RH (Table S2). Nevertheless, in IEC 5.8 samples, there is a higher number of $-SO_3H$ groups in close proximity since free acids sit in the cavities. Together, the covalently bonded and free acids reduced the inter-SO_3H distance, favorable for proton hopping in IEC 5.8 samples. Undoped calix-2 samples (IEC 2.8, 3.9) could not take advantage of such a proximal, high-density $-SO_3H$ effect. This explains why at low % RH, IEC 5.8 was the best proton conductor with a trend $(\text{calix-2})_{\text{IEC 5.8}} > (\text{calix-2})_{\text{IEC 3.9}} > (\text{calix-2})_{\text{IEC 2.8}}$ > Nafion (Figure 3c). Another important point is: Nafion films (Figure S14) sorbed water similarly or more than any calix-2 film (Figure 3d–f) but showed lower ionic conductivity (Figure 3b). In a ∼25 nm-thick film at 20–25% RH, the λ value for Nafion was ∼11, while it was ∼6 for calix-2 (IEC 3.9), but the proton conductivity was $\sim 3.1 \times 10^{-4}$ and $\sim 1.4 \times 10^{-2}$ mS/cm for the same Nafion and calix-2 films, respectively. The sorbed water in Nafion films is known to form ill-connected[10,108] ionic domains. Also, these domains have an average diameter of ∼2.2–2.3 nm (Figure S12a,b) which was not small enough to leverage the 1D water wire effect (unlike calix-2). All of these explain the low proton conductivity of Nafion thin films despite higher water uptake.

Morphology and Self-Assembly

As mentioned earlier, the added advantage of using macrocycle-based amphiphiles is that, unlike linear amphiphiles, they can spontaneously self-assemble in both solution and solid-state above the critical aggregation concentration [∼0.05 wt % for calix-2 (Figure S15)].[73,86,109] Such self-assembly can give rise to interesting architectures (vesicular, cylindrical, micellar, capsules, and more)[73,86−89] with a high level of order and connectivity[73,86] between macrocyclic cavities. This connectivity can be highly beneficial for attaining long-range ion-conduction pathways. Figure 4 shows the AFM images of ∼35–40 nm-thick films of Nafion and calix-2 at ambient humidity. While Nafion films were almost featureless (Figure 4a–c), calix-2 films formed ellipsoidal features (Figures 4d–l, S16, and S17) which was in agreement with many experimental studies on calix[n]arene-based molecules.[73,86,88,89,109] Molecular dynamics simulations of calix[n]-arene-based molecules can form multiple bilayer-like arrangements (similar to lipid bilayer membranes),[73,86,88,89,109] or simply stack in multiple layers (like a stack of cups).[90,91] In a bilayer-like arrangement, the calix[4]arene units tend to sit in an up-and-down fashion to bring similar functional groups of the rims close and directed to each other.[73,86,88,89,109] Such arrangement was commonly seen in calix[n]arene-based monomers having carboxylate,[73,89] sulfonate,[86,89,109] and phosphonate[88,89] functionalities at one rim and alkoxy chains at the other rim. On the other hand, in the stack-of-cup format,

https://doi.org/10.1021/jacsau.2c00143
JACS Au 2022, 2, 1144−1159

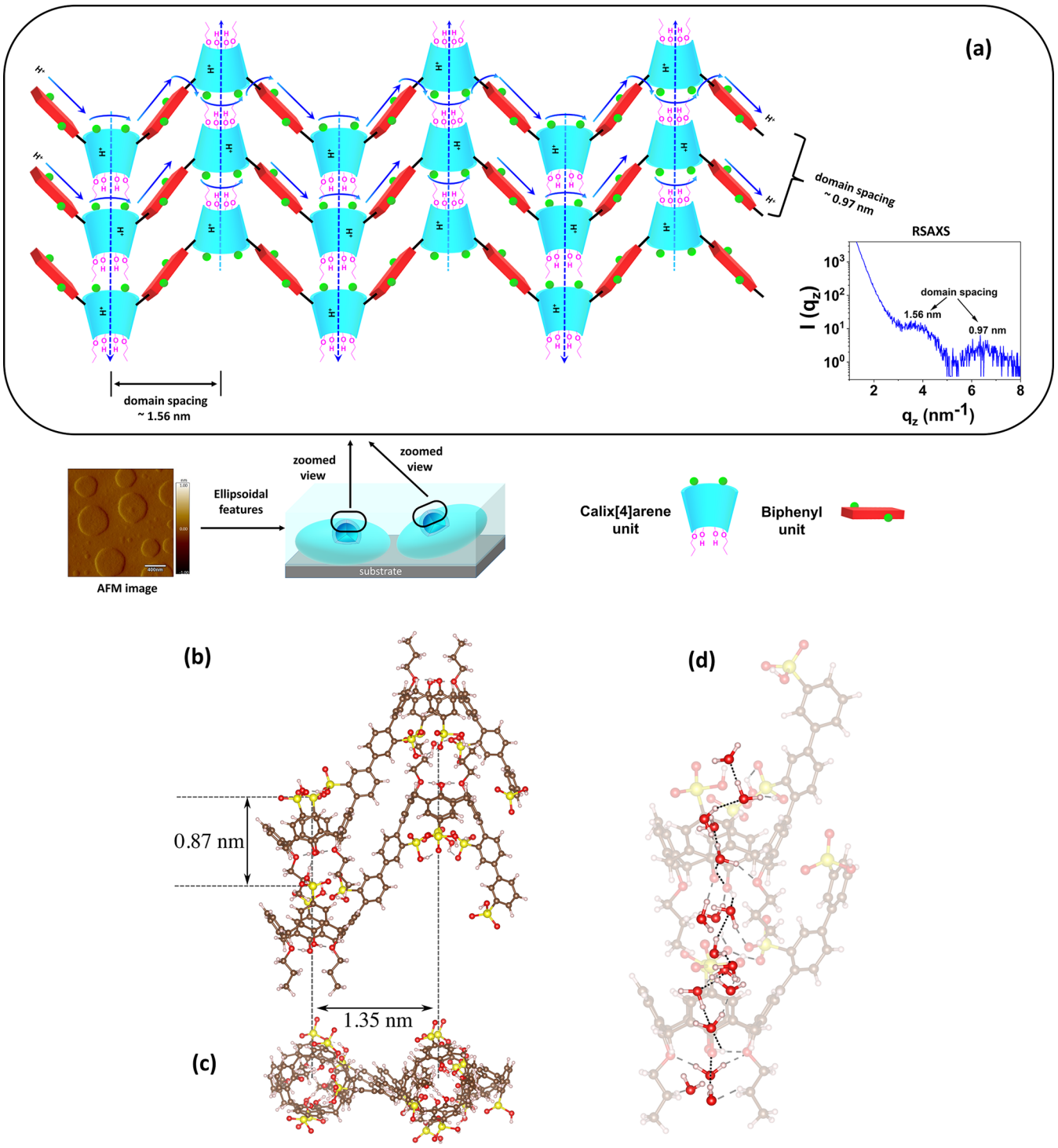

Figure 5. (a) Out-of-plane RSAXS of calix-2 (IEC 3.9) film at 92% RH (a, top, right). Proposed self-assembly modes and ionic conduction pathways within calix-2 ionomer films based on AFM and RSAXS data. The solid blue arrows represent surface proton hopping, while the dotted blue arrows represent the proton conduction across individual macrocyclic cavities and self-assembled ion channels through multiple cavities. The green balls appended to calix[4]arene and biphenyl units represent sulfonic acid ($-SO_3H$) groups. (b–d) Side (b) and top (c) views of anhydrated structural model of calix-2 ionomers comprising four calix[4]arene monomers, as identified in DFT-B3LYP calculations with characteristic domain spacings. (d) corresponds to the hydrated model with a one-dimensional chain of H-bonded water molecules. In the hydrated model, the characteristic distances are increased from ∼0.87 to ∼1 nm and from ∼1.35 to ∼1.4 nm. The atoms O, S, C, and H are represented by the colors red, yellow, brown, and white, respectively, in the atomistic simulation.

the upper rim of a calix[*n*]arene unit of one chain faced the lower rim of the calix[*n*]arene unit of the neighboring chain, which are stacked on top of each other. Such a stack-of-cup format was reported for calix[*n*]arene-phenylene-based oligo/polymers.[90,91] Primarily, the difference in these two orientations appeared to originate from the absence/presence of the phenylene-based repeat units in the chain imposing some steric stringencies (*e.g.*, maintaining an angle of 120° between 3 sp^2-

https://doi.org/10.1021/jacsau.2c00143
JACS Au 2022, 2, 1144–1159

carbons[110]). It was also shown that the stacks of calix[*n*]arene units of the polymer chains were stabilized *via* multiple interactions, such as van der Waals and hydrogen-bonding interactions.[90,91] In our case, calix-2 has sulfonic acid ($-SO_3H$) groups at the upper rims, while it has hydroxyl ($-OH$) and propoxy [$-O-(CH_2)_2-CH_3$] groups at the lower rims of calix[4]arene units. Also, the sulfonated calix[4]arene units are alternated with sulfonated biphenyl units in calix-2. Therefore, stack-of-cup conformation can be a more probable conformation for calix-2, which we confirmed later *via* atomistic simulations.

Based on the three-dimensional AFM images (Figure S16) and corresponding height profiles (Figure S17), the dimensions [$(dia)_{long\ axis} \times (dia)_{short\ axis}$] of the ellipsoidal features in calix-2 films were ∼100 nm × 50 nm and ∼500 nm × 50 nm for IEC 2.8 and 3.9 samples, respectively. IEC 5.8 samples showed more polydispersity in the size of the features with a mix of both large (∼500 nm × 120−160 nm) and small (∼500 nm × 20−40 nm) ellipsoids. The gradually increasing feature size with IEC was consistent with the trends observed for other ionomers.[23] The dimensions of ellipsoidal features also suggested that the calix-2 films likely had ∼20−80 layers of calix[4]arenes stacked within each spheroidal feature based on the calculation of the height of one calix[4]arene unit in a stack (∼1.0 nm). Such stacked arrangement can give rise to ionic conduction pathways with multiple length scales: (i) across individual calix[4]arene units of calix-2 (molecular-level ion channels), (ii) across overlapped/aligned macrocyclic units in a stack (connected ion channels), and (iii) along the surface of the upper rims of calix[4]arene units where the $-SO_3H$ groups are sitting side-by-side (lateral proton hopping along the chains). The presence of such multilength scale ionic domains was further confirmed through reflection small-angle X-ray scattering (RSAXS) and atomistic simulations.

We performed both in-plane and out-of-plane RSAXS of ∼136 nm-thick calix-2 (IEC 3.9) films. RSAXS, a special type of grazing incidence small-angle X-ray scattering (GISAXS), uses a point detector (0D approach) to capture the scattering intensity in-plane (q_p) or out-of-plane (q_z) direction at a time. We did not see any scattering in the in-plane direction, but we saw two prominent scattering peaks in the out-of-plane direction (Figure 5a, right). Although the origin of the absence of the in-plane scattering peak was unclear, it was evident that there were repeating structures in the out-of-plane or *z*-direction. The situation can be imagined better with an example of lamellar sheets (seen in block copolymers[111]), where the conducting lamella repeating in the *z*-direction act like proton-conduction pathways along the in-plane direction.

The two out-of-plane scattering peaks for the calix-2 (IEC 3.9) film were seen at q_z values of 4.02 nm^{-1} (*d*-spacing ∼1.56 nm) and 6.46 nm^{-1} (*d*-spacing ∼0.97 nm), suggesting the presence of two ordered/repeating structures in the *z*-direction. The *d*-spacing of ∼1.56 nm for the first scattering peak could be attributed to the ionic domains through the macrocyclic cavities of calix[4]arene repeat units. We made this assignment since the theoretically calculated distance between two macrocyclic repeat units, spaced by a biphenyl unit in a calix-2 chain, is ∼1.56 nm. The other domain spacing (0.97 nm) was likely a spacing between two consecutive lateral proton-hopping sites, which was equivalent to the width of a single layer (calculated theoretically as ∼1.0 nm). This suggested that the macrocyclic units were aligned and acted like ion-conducting channels/domains across the stacks of macrocycles. Because of the bond angle constraints,[110] the ion-conducting channels across macrocycle axes (∼1.56 nm) and the lateral proton-hopping pathways (0.97 nm) from the same ellipsoidal aggregate cannot be oriented along the same direction. This suggested that the two peaks in the out-of-plane scattering (Figure 5a, right) were likely captured from two most repeating domain spacings from two differently oriented ellipsoids. We thus reasonably approximated that in our films, there was likely a distribution of orientations of ellipsoidal features with respect to the substrate (*e.g.*, some ellipsoids were sitting parallel to the substrate, and some were not). Now, due to the film thickness constraints (30−150 nm), ellipsoids (with dimension 500 nm × 50 nm in IEC 3.9 samples) might find it difficult to stand with their long axis completely perpendicular to the substrate. Otherwise, we would have seen some very large dimensions in the height direction in the height *versus* width plots (Figure S17). Therefore, chances are that a fraction of ellipsoids were lying with their long axis parallel to the substrate, and another fraction of ellipsoids were slanting with the substrate. The top panel of Figure 5a represents the self-assembly mode and chain packing parallel to the long axis of the ellipsoids. Please note that this chain packing is shown irrespective of the orientation of the ellipsoids with respect to the substrate in the calix-2 (IEC 3.9) film. Here, the ion-conducting pathways created by the alignment of macrocyclic cavities are shown in dotted blue arrows, while the surface proton hopping, happening along the calix-2 chains, is shown by solid blue arrows.

The distribution of ellipsoids [parallel to the substrate and slant with the substrate but not likely perpendicular to the substrate (Figure 5a)], predicted from RSAXS and AFM data, also corroborated with the proton conductivity values. Calix-2 chains are not linear. Due to the inter-repeat unit bond angle and curvature of the ellipsoids, it can thus be imagined that some calix cavities from the stacked chains in surface-slant ellipsoids can certainly be along the in-plane proton transport pathways. On the other hand, the out-of-plane conductivity should have been very high if all ellipsoids were stacked parallel to the substrate (*i.e.*, all calix cavities were along the out-of-plane proton transport pathway). Due to the likelihood of such distribution of the alignment angle of ellipsoids, both in-plane and out-of-plane conductivity may have components of through-chain transport (along $-SO_3H$ groups) and through-cavity transport.

Atomistic Simulations

To provide the mechanistic insights into the experimental findings, support the self-assembly proposed in Figure 5a, and show whether cavity-level transport is favorable, we performed a set of atomistic simulations (Figure 5b−d). First, the classical MMFF94s force field in the Avogadro package[112,113] was employed to preoptimize two plausible calix-2 ionomer structures composed of four sulfonated, calix[4]arene-biphenyl-based monomeric repeat units. The size of these ionomer fragments was chosen to be small enough for subsequent calculations within the density functional theory (DFT) approach using the B3LYP functional. We then commenced DFT optimizations of both structures using the NWChem[114] computational chemistry package (see the Computational Details section) to identify the structure shown in Figure 5b−d as the most stable. This structure was characterized by almost a straight line connecting phenyl rings of calix[4]arene units through biphenyl rings, thus rendering

https://doi.org/10.1021/jacsau.2c00143
JACS Au 2022, 2, 1144−1159

small stress in the polymerized structure. This also showed a good alignment of calix[4]arene units creating stacks of macrocycles. It is to be noted that these simulations were carried out for the maximum sulfonation of the ionomer corresponding to IEC ∼4. Here, we considered both nonhydrated (Figure 5b,c) and hydrated (Figure 5d) models. In the hydrated model, we only populated the one-dimensional channels with enough water molecules so that they can potentially form a H-bonded water wire. It can be seen in the figure that the computed characteristic distances are in reasonable agreement with experimentally measured domain spacings, being expectedly smaller for the anhydrated (∼0.87, ∼1.35 nm) and relatively larger for the hydrated (∼1, ∼1.4 nm) models. This is in close agreement with RSAXS data and the proposed self-assembly (Figure 5a). Moreover, we observed the formation of H-bonded water wires inside the calix channels, with hydrogen bonds being in the range of about 1.44−1.8 Å. While much more expensive molecular dynamics simulations could provide more detailed information on the distribution of H-bond distances, our static calculations supported the possibility of H-bonded water wire formation in the channels that should promote proton transfer. Also, during DFT optimizations, we observed spontaneous proton transfer from $-SO_3H$ groups to H_2O species inside the channels to yield H_3O^+. Such continuous pathways and 1D water wire can effectively minimize the local proton accumulation, an issue of conventional ionomers in thin films.[28,115]

Through-Plane Proton Conduction Profile

The confocal laser scanning microscopy (CLSM) imaging of a Nafion−calix-2 composite film (Figure 6) provided a strong

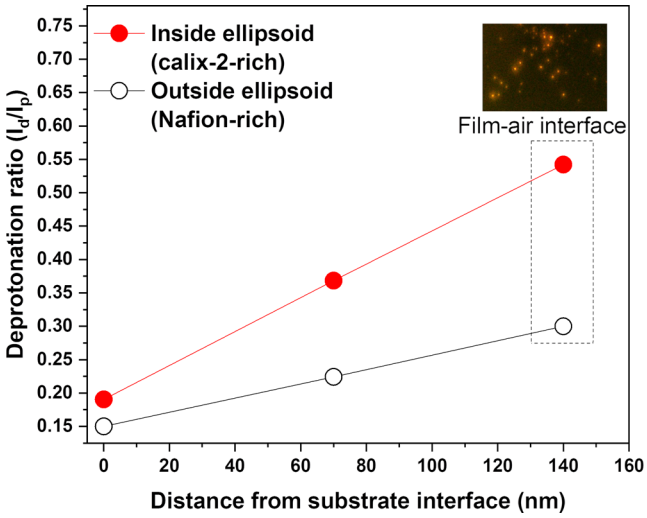

Figure 6. Through-plane proton conduction (I_d/I_p) profile of a Nafion−calix-2 composite film (∼140 nm thick) at 80% RH. The inset shows the CLSM image of the film at the film−air interface (scale bar 1 μm). The I_d/I_p values at this film−air interface are shown within the dotted black box. Here, the IEC of the calix-2 used to make the film was 3.9.

experimental evidence of the role of macrocyclic cavities on proton conduction. In our prior work,[7] we have demonstrated this CLSM-based strategy to reveal a through-plane (*z*-direction) proton conduction profile across ionomer films. By now, we know that calix-2 forms ellipsoidal features, while Nafion makes featureless films (AFM images, Figure 4). Therefore, if a Nafion−calix-2 composite film is made, an ellipsoidal feature in that film can be located and through-plane proton conduction across that ellipsoidal feature (*i.e.*, across calix cavity-rich region) can be measured using CLSM. Also, a featureless region (Nafion-rich) can be located and through-plane proton conduction across that region can be measured. Therefore, CLSM imaging of the Nafion−calix-2 film can give us a visual of how different the proton conductivity is at the positions in a film where calix-2 units are located as compared to the places with no cavity-forming units.

CLSM-based through-plane proton conduction study was made possible by incorporating a proton concentration-sensitive, fluorescent photoacid probe (8-hydroxypyrene-1,3,6-trisulfonic acid, trisodium salt, HPTS, Figure S18) into the film. Incorporating photoacid probes within polymeric systems has been proven to be very helpful to reveal information about the proton conduction environment, such as the extent of proton conduction,[7,28,115] proton transport dynamics,[116−119] and more. In a way, the photoacid dye HPTS behaves just like an ionomer. In brief, HPTS, in a favorable proton conduction environment, emits fluorescence from its deprotonated state (I_d, λ_{em} ∼ 510 nm) more than its protonated state (I_p, λ_{em} ∼ 430 nm). The deprotonation ratio (I_d/I_p) thus becomes higher at locations within a film where proton conduction is stronger. Therefore, we can generate a through-plane proton conduction profile along any vertical plane of our interest within a film by capturing I_d/I_p at different depths along that plane. It is to be noted that the CLSM image was created by superpositioning the emission of deprotonated (I_d) and protonated (I_p) states of HPTS. Also, since it is difficult to distinguish between blue and green colors by naked eyes, the red and green in the images were pseudocolors representing I_d and I_p, respectively.

As expected from the AFM images (Figure 4), we saw ellipsoidal features (calix-2 rich region) surrounded by featureless (Nafion-rich) regions in the CLSM image of the Nafion−calix-2 composite film (Figure 6, inset). We also saw that the proton conduction was better at places within a film where macrocycles were located. At the air interface, the calix-2-rich regions showed bright reddish-orange dots, while the Nafion-rich regions showed weaker orange fluorescence (Figure 6, insets). The bright-reddish orange color was a sign of predominance of strong proton conduction in calix-2 rich regions. The proton conduction profile along the *z*-direction (Figure 6) also showed that the deprotonation ratio (I_d/I_p) at a point over the ellipsoidal feature (calix-2 rich) was ∼3 times higher than that at a point outside of the ellipsoidal feature (*i.e.*, Nafion-rich region). This indicated that the proton conduction through the macrocyclic cavities is the reason behind higher proton conductivity of calix-2-containing films.

While proving molecular-level or single-cavity-level proton conduction is difficult, this specific experiment allowed us to locate fluorescent dyes inside the cavities. This can be said with certainty as macrocyclic cavities are by nature more prone to capture dyes[90,120−122] and thus are frequently employed for dye removal in environmental applications.[90] Since we were able to trap the HPTS dyes within the macrocyclic cavities and these dyes showed bright reddish-orange color with a higher I_d/I_p value (Figure 6), it was more evident that the molecular cavities caused strong proton transport.

Proton Conductivity in Bulk Membrane

We were also able to cast transparent Nafion−calix-2 composite membranes (Figure 7, inset) with different

https://doi.org/10.1021/jacsau.2c00143
JACS Au 2022, 2, 1144−1159

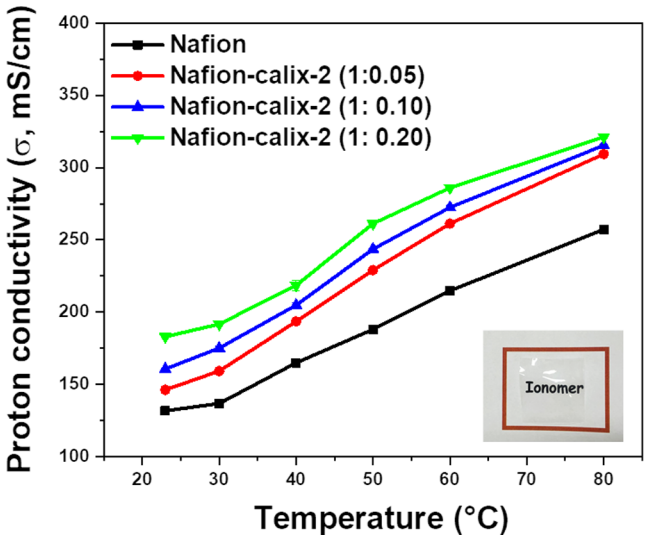

Figure 7. Proton conductivities of bulk Nafion and Nafion−calix-2 (IEC 3.9) composite membranes with different Nafion-to-calix-2 ratios. The thickness of the membranes ranged between 60 and 70 μm. The measurements were taken from 23 to 80 °C in bulk water. The inset shows a photograph of a Nafion−calix-2 composite membrane.

Nafion-to-calix-2 ratios. The calix-2 ionomer not only did improve the proton conductivity of sub-micrometer-thick films (Figure 3a−c) but also improved the proton conductivity of several tens of micrometer-thick bulk, free-standing membranes (Figure 7). At a very low loading of calix-2 within the Nafion matrix [Nafion−calix-2 = 1:0.20 (w/w)], the proton conductivity of the composite membrane (σ_m) was 321 mS/cm, while it was 257 mS/cm for the pure Nafion membrane in bulk water at 80 °C (Figure 7). Even when we made Nafion and Nafion−calix-2 composite membranes by keeping the total number of moles of $-SO_3H$ constant, the Nafion−calix-2 [Nafion−calix-2 = 1:0.17 (w/w)] composite membrane showed conductivity higher than Nafion (Figure S19a). This again pointed toward the role of sub-nanometer, macrocyclic cavity-forming units in improving the proton conductivity of membranes. It is also to be noted that high proton conductivity over a range of relative humidity conditions is desired for both low- and high-temperature fuel cells.[97] Achieving high conductivity at low % RH becomes especially critical for high-temperature fuel cell operations as water tends to evaporate. We saw that the Nafion−calix-2 composite membrane [~6 mS/cm, Nafion−calix-2 = 1:0.10 (w/w)] offered improved conductivity over the Nafion membrane (~3 mS/cm) under high temperature (70 °C)−low humidity (30% RH) conditions.

It is to be noted that to make Nafion−calix-2 composite membranes, we had to prepare separate stock solutions of Nafion and calix-2. Later, the stock solutions were mixed together to cast the composite membranes. When we did AFM of Nafion−calix-2 composites (Figure S19b−d), we saw ellipsoidal features with dimensions similar to what we saw in AFM images of pure calix-2 films (Figure 4g−i). This proved that the self-assembly of calix-2 into ellipsoidal features happened in solution and was retained in the film/membrane no matter whether it was pure calix-2 or calix-2 in a Nafion matrix.

We also measured the time-dependent proton permeation across Nafion−calix-2 composite membranes in comparison with the pure Nafion membrane. The measurements were done at two different concentration gradients of HCl [1 M (Figure 8a) and 3 M (Figure 8b)] across feed and reservoir

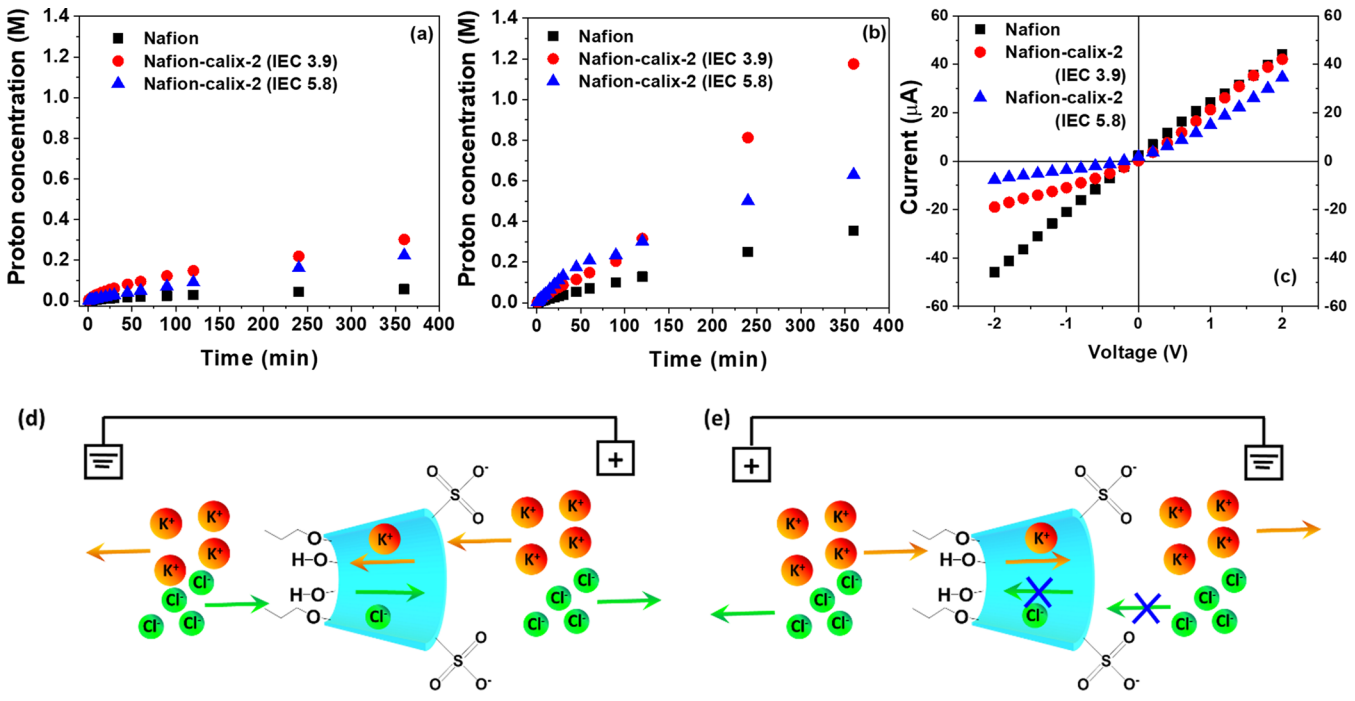

Figure 8. Time-dependent proton permeation (measured as proton concentration in the receiving compartment) through pure Nafion and Nafion−calix-2 composite membranes at 1 M (a) and 3 M HCl (b). (c) *I*−*V* curves of Nafion and Nafion−calix-2 (IEC 3.9 and IEC 5.8) composite membranes were recorded in 0.1 M KCl in DI water. (d,e) Schematic illustration of ionic current direction across a macrocyclic unit in the composite membranes at different applied voltages [forward (d) and reverse (e) biases].

https://doi.org/10.1021/jacsau.2c00143
JACS Au 2022, 2, 1144−1159

compartments (Figure S20 for experimental setup). Having a trace amount of calix-2 within the Nafion membrane matrix [Nafion−calix-2 = 1:0.05 (w/w)] made the proton permeation through the bulk composite membranes much faster in comparison to pure Nafion membranes. The faster proton permeation in the presence of calix-2 within the membrane again demonstrated the potential of calix-2 to create unique and efficient proton conduction pathways across macrocyclic cavities.

Voltage Gating

The calix-2 ionomers also acted like ionic diodes (like nature-mimicking and Janus systems[37−42]) and controlled the direction of ion passage as the macrocyclic repeat units had an asymmetric distribution of ionic groups between the upper ($-SO_3H$) and lower [$-OH$, $-O-(CH_2)_2-CH_3$] rims. The calix-2-containing Nafion membranes showed voltage-dependent gating behavior, where different ionic currents were observed when forward and reverse bias voltages of the same magnitude (−2 to +2 V) were applied (Figure S21 for experimental setup). Nafion−calix-2 composite membranes took advantage of the asymmetric charge distribution across calix[4]arene units and exhibited voltage-gating behavior with rectification ratios ($|I_{+2V}/I_{-2V}|$) of ∼2.21 (IEC 3.9) and ∼4.55 (IEC 5.8) (Figure 8). Here, at positive bias, the applied electric field drove the transport of K^+ ions along the axes of calix[4]arene units from the upper- to lower-rim side (Figure 8d). The $-SO_3^-$ groups at the upper rim of calix[4]arene units facilitated this cationic K^+ ion transport. At the same time, Cl^- ions were transported in the reverse direction. Such ionic transport increased the total ion concentration inside the macrocyclic ion channels and showed a high ionic current at a forward bias (Figure 8c,d). On the other hand, at negative bias, K^+ ions got transported from the lower- to the upper-rim side, but Cl^- ion transport was prevented by the anionic $-SO_3^-$ groups at the upper rim of macrocycles. As a result, the ionic current in reverse bias decreased (Figure 8c,e). The whole effect was observed as an ionic rectification ratio >1 for calix-2-based composite membranes. Here, the cup-like stacking of calix[4]arene units (lower rim of one macrocycle facing the upper rim of the next one) in an aggregate created continued pathways with asymmetric charge distribution, which was congenial for voltage gating and inhibiting local ion accumulation. The observed voltage gating or preferential ionic current was, therefore, a collective and resultant effect of local ionic movement across different calix-2 aggregates oriented in different directions within the membrane. Since such asymmetric charge distribution was not present in the pure Nafion membrane, it could not show any voltage-gating behavior and the corresponding rectification ratio was ∼1. The ionic rectification ratio of the composite membrane consisting of calix-2 (IEC 5.8) was higher than that consisting of calix-2 (IEC 3.9). This could be attributed to an increased repulsion effect on Cl^- ions in reverse bias as the additional $-SO_3^-$ groups from free acids were sitting in the cavities of calix[4]arene units in the IEC 5.8 samples.

Broader Impacts on Energy Technologies

We have shown how by incorporating sub-nanometer-sized cavities of calix[4]arene within the ionomer chemical structure, we not only can improve the thin-film proton conductivity significantly but also can achieve voltage gating-induced ion-permselective behavior. The voltage-gating behavior can have implications in water electrolysis, desalination, metal extraction for lithium-/sodium-ion batteries, and more. On the other hand, the faster passage of water and protons through such narrow cavities opens up new ways to alleviate local proton accumulation,[28,115] an issue identified with Nafion in thin films and membranes. While the macrocycle-containing ionomers can have many exciting applications, these ionomers can certainly open up new ways to design efficient electrodes for energy conversion and storage devices.[1,2] Ion transport[5,8,10,101,103−105,123] and gas transport[3,4,124,125] resistances at ionomer−catalyst interfaces are two of the major technological challenges of electrodes of fuel cells/electrolyzers. These resistances make the electrochemical reaction sluggish. The typical way to deal with these problems has by far been the development of catalysts[92,93,126−128] with large electrochemically active surface area. Here, we are trying to address these issues by designing new ionomers. If the macrocycle-containing ionomers are used as sub-micrometer-thick binders on electrodes, the molecular-level cavities of these ionomer chains can contribute to minimize ion transport resistance to a great extent. At the same time, such open structures of these ionomers might be beneficial to reduce local gas transport resistance.[3,4,124,125] Such much-needed technological improvement through ionomer binder design can transform the performance of energy conversion and storage devices.

CONCLUSIONS

By designing a nature-inspired class of ionomers (calix-2) containing macrocyclic calix[4]arene units, here, we showed how to take confinement in favor of us to improve thin-film proton conductivity. By leveraging the sub-nanometer-sized cavities of calix[4]arene (1D water wire) in calix-2, we were able to achieve up to 1−2 orders of magnitude improvement in proton conductivity as compared to the current benchmark ionomer Nafion in <100 nm-thick films. The role of macrocyclic cavities in elevating proton conductivity was confirmed through extensive synthetic, analytical (CLSM), and theoretical (atomistic simulations) efforts. The combination of AFM, GISAXS, and atomistic simulations allowed us to rationally propose the self-assembly modes in calix-2-based materials. As per these findings, the systematic calix-2 chain organization enabled formation of 1D water wires through the aligned macrocyclic cavities and facilitated long-range proton conduction in both thin films and bulk membranes. Especially, the thin-film results showed great promise of calix-2 ionomers to address and overcome the ion transport limitation at ionomer−catalyst interfaces on electrodes of fuel cells, electrolyzers, and many other electrochemical devices. Moreover, when we incorporated calix-2 within Nafion membrane matrices, the ionomer demonstrated voltage-dependent ionic current. Such voltage-gating behavior makes these ionomers a potential candidate to design bulk membranes/films with selective ion permeation and blocking capabilities.

METHODS

Ionomer Synthesis

The synthesis of monomeric intermediates (**2** and **3**) is shown in the Supporting Information. The synthetic and analytical characterization details of calixn-2 (neutral) and calix-2 ionomers are shown below:

Calixn-2

A mixture of **3** (2.6 g, 3.91 mmol), 4,4′-biphenylene bis(boronic acid) (0.943 g, 3.90 mmol), tertrakis(triphenylphosphine)palladium(0)

https://doi.org/10.1021/jacsau.2c00143
JACS Au 2022, 2, 1144−1159

(2.25 g, 1.95 mmol), anhydrous toluene (5 mL), and anhydrous methanol (0.5 mL) was stirred at 100 °C. After 15 min, potassium carbonate (2 M, 4 mL) was added to the solution and then stirred again at 100 °C for 5 days. Upon completion of the reaction, the mixture was cooled down to room temperature. The organic layer was extracted with dichloromethane (10 mL), washed with DI water (10 mL) and HCl (1 M, 10 mL), and dried using sodium sulfate. The residue was triturated with boiling diethyl ether (3 × 10 mL) to obtain calixn-2 (1.42 g, yield 53%). Molecular weight [M_n: 5022 g/mol, polydispersity index (PDI): 2.48]. ^{1}H NMR (400 MHz, $CDCl_3$): δ 1.35 (t, 6H, from $-CH_3$ of 2 $-O-CH_2-CH_2-\mathbf{CH_3}$); 2.11 (m, 4H from $-CH_2-$ of 2 $-O-CH_2-\mathbf{CH_2}-CH_3$); 3.41 (d, 4H, 1H from each $-CH_2-$ of Ar-CH_2-Ar); 4.01 (t, 4H, from each $-CH_2-$ of 2 $-O-\mathbf{CH_2}-CH_2-CH_3$); 4.35 (d, 4H, 1H from each $-CH_2-$ of Ar-CH_2-Ar); 6.67−7.73 (18H, 10H from calix[4]arene unit + 8H from biphenyl unit); 8.34 (s, 2H, −OH). ^{13}C NMR (100 MHz, $CDCl_3$): 153.40 (**Ar**-OH), 151.92 (**Ar**-OH), 133.51−118.98 (**Ar**), 78.34 ($-O-\mathbf{CH_2}-CH_2-CH_3$), 31.46 (Ar-$\mathbf{CH_2}$-Ar), 23.53 ($-O-CH_2-\mathbf{CH_2}-CH_3$), 10.96 ($-O-CH_2-CH_2-\mathbf{CH_3}$). The ^{1}H NMR and ^{13}C NMR spectra of calixn-2 are shown in Figures S5 and S6.

Calix-2

To a round-bottom flask equipped with a dropping funnel, 0.50 g of calixn-2 was added. Dry dichloromethane (10 mL) was added to the flask, and the mixture was stirred for 30 min at −20 °C. To this mixture, chlorosulfonic acid [$ClSO_3H$, 1 mL (for IEC 2.8), 1.5 mL (IEC 3.9)] in dry dichloromethane (5 mL) at −20 °C was added dropwise through a dropping funnel while the inert atmosphere was maintained, and the mixture was stirred at this temperature for 30 min. The mixture was then brought to room temperature and stirred for another 30 min. After the reaction was completed, the mixture was poured into ice-cold water, followed by ultrasonication for 2 h. This washing−sonication cycle was repeated thrice, decanting the water at the end of each cycle so that the free acids can be efficiently removed from the reaction mixture. The rest of the mixture was then washed with hexane thrice to precipitate out the compound (as brown powder). Drying this powder under vacuum at 60 °C for 10 h yielded the sulfonated **calix-2** ionomer [0.30 g, yield 49% (IEC 2.8); 0.37 g, yield 50% (IEC 3.9)]. Molecular weight: M_n 5671; M_w 13,566; PDI 2.39 (IEC 2.8); M_n 6138; M_w 20,245; PDI 3.30 (IEC 3.9).

The abovementioned sulfonation method was used to synthesize calix-2 with IEC 2.8 and 3.9. Calix-2 samples with IEC 5.8 possessed both covalently bonded $-SO_3H$ and noncovalently trapped free acids. Here is the procedure to obtain calix-2 with IEC 5.8: to 0.5 g of calixn-2 in a 50 mL round-bottom flask equipped with a magnetic stirring bar; chlorosulfonic acid ($ClSO_3H$, 5 mL) in dry dichloromethane (3 mL) at −20 °C was added dropwise for 30 min using a dropping funnel. The mixture was stirred for another hour to ensure good acid doping, then brought to room temperature and stirred for 30 min more. This high IEC calix-2 was neither soluble in dichloromethane nor completely soluble in water. The unreacted or untrapped free acids were thus removed through a multistep process. First, the ice-cold water wash (∼10 min)−sonication (2 h) cycle was repeated thrice, followed by decanting the water phase at the end of each cycle. The reaction flask was then placed into a preheated oil bath at 80 °C with stirring (200 rpm) for 4 h, which removed dichloromethane and a fraction of water. The solution (still containing some water) was then vortexed and ultrasonicated for 6 h so that the free acids (loosely captured in the macrocyclic cavities) can come out of the cavities to the remaining water phase. The dispersed solution was kept overnight inside the fume hood. This allowed the polymer phase to settle down, while the free acids still stayed in the water phase. This polymer−water biphasic system was then transferred to a dialysis pouch. The neutral calixn-2 had a M_n slightly higher than 5000. Therefore, the molecular weight cutoff of the dialysis membrane was chosen as 5000 to remove the free acids and the low MW- and water-soluble chains of calix-2. At the end of ∼72 h dialysis against DI water, the pH of the external solution was ∼3−4, which was constant for the last 12 h of the process. After dialysis, the solution was taken out of the membrane, dried in an oven, and washed with hexane several times to get a brown powder (0.4 g). Molecular weight M_n 6542; M_w 22,238; PDI 3.40.

Computational Details

Atomistic simulations were performed in two steps. First, atomic-structure optimizations of calix-2 ionomers comprising four elementary units were carried out using the MMFF94s force field in Avogadro software.[112,113] Then, the classically optimized structures were fed into the *ab initio* NWChem code (version 7.0.2) to optimize the geometries within the DFT approach.[114] Here, we first employed 3-21G and then 6-31G basis sets on all atoms in combination with the B3LYP exchange−correlation functional using the NWChem default convergence criteria. The most energetically favorable structure (see Figure 5b,c) was then used to add H_2Os species inside the calix channels. The identified H-bonded water wire that was suggested to promote H transfer inside the channels is depicted in Figure 5d.

■ ASSOCIATED CONTENT

Supporting Information

The Supporting Information is available free of charge at https://pubs.acs.org/doi/10.1021/jacsau.2c00143.

NMR, HRMS, TGA, RSAXS, EIS, AFM, and additional experimental details (PDF)

■ AUTHOR INFORMATION

Corresponding Author

Shudipto Konika Dishari − *Department of Chemical and Biomolecular Engineering, University of Nebraska−Lincoln, Lincoln 68588 Nebraska, United States;* orcid.org/0000-0003-1679-2332; Email: sdishari2@unl.edu

Authors

Shyambo Chatterjee − *Department of Chemical and Biomolecular Engineering, University of Nebraska−Lincoln, Lincoln 68588 Nebraska, United States*

Ehsan Zamani − *Department of Chemical and Biomolecular Engineering, University of Nebraska−Lincoln, Lincoln 68588 Nebraska, United States*

Seefat Farzin − *Department of Chemical and Biomolecular Engineering, University of Nebraska−Lincoln, Lincoln 68588 Nebraska, United States*

Iman Evazzade − *Department of Chemical and Biomolecular Engineering, University of Nebraska−Lincoln, Lincoln 68588 Nebraska, United States*

Oghenetega Allen Obewhere − *Department of Chemical and Biomolecular Engineering, University of Nebraska−Lincoln, Lincoln 68588 Nebraska, United States*

Tyler James Johnson − *Department of Chemical and Biomolecular Engineering, University of Nebraska−Lincoln, Lincoln 68588 Nebraska, United States*

Vitaly Alexandrov − *Department of Chemical and Biomolecular Engineering, University of Nebraska−Lincoln, Lincoln 68588 Nebraska, United States;* orcid.org/0000-0003-2063-6914

Complete contact information is available at: https://pubs.acs.org/10.1021/jacsau.2c00143

Author Contributions

†S.C., E.Z., and S.F. contributed equally to this work.

Notes

The authors declare no competing financial interest.

https://doi.org/10.1021/jacsau.2c00143
JACS Au 2022, 2, 1144−1159

■ ACKNOWLEDGMENTS

The research was primarily supported by the U.S. Department of Energy (DOE), Office of Science, Basic Energy Sciences (BES), under award # DE-SC0020336 (oligomeric and gated calix-2 ionomer synthesis, as well as scattering, morphology, proton permeation, and voltage-gating studies). Thin-film studies of Nafion and development of CLSM-based strategy were supported by the National Science Foundation (NSF) CAREER Award (NSF-DMR # 1750040). S.K.D. also acknowledges the support from the NSF CAREER Award for purchasing the EIS instrument. S.C., E.Z., S.F., and O.A.O. acknowledge partial supports from the NSF (NSF-DMR # 1750040), DOE (DE-SC0020336), and Nebraska Center for Energy Science Research (NCESR). S.K.D. thanks Dr. Kevin G. Yager (Brookhaven National Laboratory) for insightful discussion on interpreting the RSAXS data. Part of this research (DSC, TGA, RSAXS, SE, XPS, and nanofabrication) was performed in the Nebraska Nanoscale Facility: National Nanotechnology Coordinated Infrastructure and the Nebraska Center for Materials and Nanoscience, which are supported by the National Science Foundation under award NNCI-1542182, and the Nebraska Research Initiative. The CLSM images were taken at the Microscopy Core Facility of the Nebraska Center for Biotechnology. The authors also thank the Nano-Engineering Research Core Facility (NERCF) at the UNL for AFM studies of ionomeric materials.

■ REFERENCES

(1) Cullen, D. A.; Neyerlin, K. C.; Ahluwalia, R. K.; Mukundan, R.; More, K. L.; Borup, R. L.; Weber, A. Z.; Myers, D. J.; Kusoglu, A. New Roads and Challenges for Fuel Cells in Heavy-Duty Transportation. *Nat. Energy* **2021**, *6*, 462−474.
(2) Gittleman, C. S.; Jia, H.; De Castro, E. S.; Chisholm, C. R. I.; Kim, Y. S. Proton Conductors for Heavy-Duty Vehicle Fuel Cells. *Joule* **2021**, *5*, 1660−1677.
(3) Kongkanand, A.; Mathias, M. F. The Priority and Challenge of High-Power Performance of Low-Platinum Proton-Exchange Membrane Fuel Cells. *J. Phys. Chem. Lett.* **2016**, *7*, 1127−1137.
(4) Gittleman, C. S.; Kongkanand, A.; Masten, D.; Gu, W. Materials Research and Development Focus Areas for Low Cost Automotive Proton-Exchange Membrane Fuel Cells. *Curr. Opin. Electrochem.* **2019**, *18*, 81−89.
(5) Holdcroft, S. Fuel Cell Catalyst Layers: A Polymer Science Perspective. *Chem. Mater.* **2014**, *26*, 381−393.
(6) Kusoglu, A.; Weber, A. Z. New Insights into Perfluorinated Sulfonic-Acid Ionomers. *Chem. Rev.* **2017**, *117*, 987−1104.
(7) Farzin, S.; Zamani, E.; Dishari, S. K. Unraveling Depth-Specific Ionic Conduction and Stiffness Behavior across Ionomer Thin Films and Bulk Membranes. *ACS Macro Lett.* **2021**, *10*, 791−798.
(8) Karan, K. Interesting Facets of Surface, Interfacial, and Bulk Characteristics of Perfluorinated Ionomer Films. *Langmuir* **2019**, *35*, 13489−13520.
(9) Hwang, M.; Nixon, K.; Sun, R.; Willis, C.; Elabd, Y. A. Sulfonated Pentablock Terpolymers as Membranes and Ionomers in Hydrogen Fuel Cells. *J. Membr. Sci.* **2021**, *633*, 119330.
(10) Modestino, M. A.; Paul, D. K.; Dishari, S.; Petrina, S. A.; Allen, F. I.; Hickner, M. A.; Karan, K.; Segalman, R. A.; Weber, A. Z. Self-Assembly and Transport Limitations in Confined Nafion Films. *Macromolecules* **2013**, *46*, 867−873.
(11) Asano, N.; Aoki, M.; Suzuki, S.; Miyatake, K.; Uchida, H.; Watanabe, M. Aliphatic/Aromatic Polyimide Ionomers as a Proton Conductive Membrane for Fuel Cell Applications. *J. Am. Chem. Soc.* **2006**, *128*, 1762−1769.
(12) Chang, Y.; Brunello, G. F.; Fuller, J.; Disabb-Miller, M. L.; Hawley, M. E.; Kim, Y. S.; Hickner, M. a.; Jang, S. S.; Bae, C. Polymer Electrolyte Membranes Based on Poly(Arylene Ether Sulfone) with Pendant Perfluorosulfonic Acid. *Polym. Chem.* **2013**, *4*, 272−281.
(13) Adamski, M.; Peressin, N.; Holdcroft, S. On the Evolution of Sulfonated Polyphenylenes as Proton Exchange Membranes for Fuel Cells. *Mater. Adv.* **2021**, *2*, 4966−5005.
(14) Chang, Y.; Mohanty, A. D.; Smedley, S. B.; Abu-Hakmeh, K.; Lee, Y. H.; Morgan, J. E.; Hickner, M. A.; Jang, S. S.; Ryu, C. Y.; Bae, C. Effect of Superacidic Side Chain Structures on High Conductivity Aromatic Polymer Fuel Cell Membranes. *Macromolecules* **2015**, *48*, 7117−7126.
(15) Elabd, Y. A.; Hickner, M. A. Block Copolymers for Fuel Cells. *Macromolecules* **2011**, *44*, 1−11.
(16) Yandrasits, M.; Lindell, M.; Schaberg, M.; Kurkowski, M. Increasing Fuel Cell Efficiency by Using Ultra-Low Equivalent Weight Ionomers. *Electrochem. Soc. Interface* **2017**, *26*, 49−53.
(17) Hickner, M. A.; Pivovar, B. S. The Chemical and Structural Nature of Proton Exchange Membrane Fuel Cell Properties. *Fuel Cells* **2005**, *5*, 213−229.
(18) Astill, T.; Xie, Z.; Shi, Z.; Navessin, T.; Holdcroft, S. Factors Influencing Electrochemical Properties and Performance of Hydrocarbon-Based Electrolyte PEMFC Catalyst Layers. *J. Electrochem. Soc.* **2009**, *156*, B499−B508.
(19) Dishari, S. Current Understanding of Proton Conduction in Confined Ionomeric Systems. *J. Postdoc. Res.* **2014**, *2*, 30−39.
(20) Peron, J.; Shi, Z.; Holdcroft, S. Hydrocarbon Proton Conducting Polymers for Fuel Cell Catalyst Layers. *Energy Environ. Sci.* **2011**, *4*, 1575−1591.
(21) Hickner, M. A.; Ghassemi, H.; Kim, Y. S.; Einsla, B. R.; McGrath, J. E. Alternative Polymer Systems for Proton Exchange Membranes (PEMs). *Chem. Soc. Rev.* **2004**, *104*, 4587−4612.
(22) Varcoe, J. R.; Atanassov, P.; Dekel, D. R.; Herring, A. M.; Hickner, M. A.; Kohl, P. A.; Kucernak, A. R.; Mustain, W. E.; Nijmeijer, K.; Scott, K.; Xu, T.; Zhuang, L. Anion-Exchange Membranes in Electrochemical Energy Systems. *Energy Environ. Sci.* **2014**, *7*, 3135−3191.
(23) Farzin, S.; Johnson, T. J.; Chatterjee, S.; Zamani, E.; Dishari, S. K. Ionomers From Kraft Lignin for Renewable Energy Applications. *Front. Chem.* **2020**, *8*, 1−17.
(24) Lim, K. H.; Lee, A. S.; Atanasov, V.; Kerres, J.; Park, E. J.; Adhikari, S.; Maurya, S.; Manriquez, L. D.; Jung, J.; Fujimoto, C.; Matanovic, I.; Jankovic, J.; Hu, Z.; Jia, H.; Kim, Y. S. Protonated Phosphonic Acid Electrodes for High Power Heavy-Duty Vehicle Fuel Cells. *Nat. Energy* **2022**, *7*, 248−259.
(25) Venugopalan, G.; Bhattacharya, D.; Kole, S.; Ysidron, C.; Angelopoulou, P. P.; Sakellariou, G.; Arges, C. G. Correlating High Temperature Thin Film Ionomer Electrode Binder Properties to Hydrogen Pump Polarization. *Mater. Adv.* **2021**, *2*, 4228−4234.
(26) Dishari, S. K.; Hickner, M. A. Antiplasticization and Water Uptake of Nafion Thin Films. *ACS Macro Lett.* **2012**, *1*, 291−295.
(27) Dishari, S. K.; Rumble, C. A.; Maroncelli, M.; Dura, J. A.; Hickner, M. A. Unraveling the Complex Hydration Behavior of Ionomers under Thin Film Confinement. *J. Phys. Chem. C* **2018**, *122*, 3471−3481.
(28) Dishari, S. K.; Hickner, M. A. Confinement and Proton Transfer in Nafion Thin Films. *Macromolecules* **2013**, *46*, 413−421.
(29) Divekar, A. G.; Buggy, N. C.; Dudenas, P. J.; Kusoglu, A.; Seifert, S.; Pivovar, B. S.; Herring, A. M. Thin Film Morphological Characteristics of a Perfluorinated Anion Exchange Membrane. *ECS Trans.* **2019**, *92*, 715−722.
(30) Luo, X.; Kushner, D. I.; Li, J.; Park, E. J.; Kim, Y. S.; Kusoglu, A. Anion Exchange Ionomers: Impact of Chemistry on Thin-Film Properties. *Adv. Funct. Mater.* **2021**, *31*, 2008778.
(31) Chowdhury, A.; Bird, A.; Liu, J.; Zenyuk, I. V.; Kusoglu, A.; Radke, C. J.; Weber, A. Z. Linking Perfluorosulfonic Acid Ionomer Chemistry and High-Current Density Performance in Fuel-Cell Electrodes. *ACS Appl. Mater. Interfaces* **2021**, *13*, 42579−42589.
(32) Farzin, S.; Sarella, A.; Yandrasits, M. A.; Dishari, S. K. Fluorocarbon-Based Ionomers with Single Acid and Multiacid Side

Chains at Nanothin Interfaces. *J. Phys. Chem. C* **2019**, *123*, 30871−30884.
(33) Hsu, W. Y.; Gierke, T. D. Ion Transport and Clustering in Nafion Perfluorinated Membranes. *J. Membr. Sci.* **1983**, *13*, 307−326.
(34) Tunuguntla, R. H.; Allen, F. I.; Kim, K.; Belliveau, A.; Noy, A. Ultrafast Proton Transport in Sub-1 Nm Diameter Carbon Nanotube Porins. *Nat. Nanotechnol.* **2016**, *11*, 639−644.
(35) Köfinger, J.; Hummer, G.; Dellago, C. Single-File Water in Nanopores. *Phys. Chem. Chem. Phys.* **2011**, *13*, 15403−15417.
(36) Murata, K.; Mitsuoka, K.; Hirai, T.; Walz, T.; Agre, P.; Heymann, J. B.; Engel, A.; Fujiyoshi, Y. Structural Determinants of Water Permeation through Aquaporin-1. *Nature* **2000**, *407*, 599−605.
(37) Guo, Y.; Huang, H.; Li, Z.; Wang, X.; Li, P.; Deng, Z.; Peng, X. Sulfonated Sub-Nanochannels in a Robust MOF Membrane: Harvesting Salinity Gradient Power. *ACS Appl. Mater. Interfaces* **2019**, *11*, 35496−35500.
(38) Tunuguntla, R. H.; Zhang, Y.; Henley, R. Y.; Yao, Y. C.; Pham, T. A.; Wanunu, M.; Noy, A. Enhanced Water Permeability and Tunable Ion Selectivity in Subnanometer Carbon Nanotube Porins. *Science* **2017**, *357*, 792−796.
(39) Yang, H. C.; Xie, Y.; Hou, J.; Cheetham, A. K.; Chen, V.; Darling, S. B. Janus Membranes: Creating Asymmetry for Energy Efficiency. *Adv. Mater.* **2018**, *30*, 1801495.
(40) Zhang, Z.; Sui, X.; Li, P.; Xie, G.; Kong, X.-Y.; Xiao, K.; Gao, L.; Wen, L.; Jiang, L. Ultrathin and Ion-Selective Janus Membranes for High-Performance Osmotic Energy Conversion. *J. Am. Chem. Soc.* **2017**, *139*, 8905−8914.
(41) Guo, W.; Tian, Y.; Jiang, L. Asymmetric Ion Transport through Ion-Channel-Mimetic Solid-State Nanopores. *Acc. Chem. Res.* **2013**, *46*, 2834−2846.
(42) Sakai, N.; Matile, S. Synthetic Ion Channels. *Langmuir* **2013**, *29*, 9031−9040.
(43) Porter, C. J.; Werber, J. R.; Zhong, M.; Wilson, C. J.; Elimelech, M. Pathways and Challenges for Biomimetic Desalination Membranes with Sub-Nanometer Channels. *ACS Nano* **2020**, *14*, 10894−10916.
(44) Kaucher, M. S.; Peterca, M.; Dulcey, A. E.; Kim, A. J.; Vinogradov, S. A.; Hammer, D. A.; Heiney, P. A.; Percec, V. Selective Transport of Water Mediated by Porous Dendritic Dipeptides. *J. Am. Chem. Soc.* **2007**, *129*, 11698−11699.
(45) Le Duc, Y.; Michau, M.; Gilles, A.; Gence, V.; Legrand, Y.-M.; van der Lee, A.; Tingry, S.; Barboiu, M. Imidazole-Quartet Water and Proton Dipolar Channels. *Angew. Chem., Int. Ed.* **2011**, *50*, 11366−11372.
(46) Iqbal, K. S. J.; Cragg, P. J. Transmembrane Ion Transport by Calixarenes and Their Derivatives. *Dalton Trans.* **2007**, 26−32.
(47) Si, W.; Chen, L.; Hu, X.-B.; Tang, G.; Chen, Z.; Hou, J.-L.; Li, Z.-T. Selective Artificial Transmembrane Channels for Protons by Formation of Water Wires. *Angew. Chem., Int. Ed.* **2011**, *50*, 12564−12568.
(48) Shen, Y.-x.; Si, W.; Erbakan, M.; Decker, K.; De Zorzi, R.; Saboe, P. O.; Kang, Y. J.; Majd, S.; Butler, P. J.; Walz, T.; Aksimentiev, A.; Hou, J.-L.; Kumar, M. Highly Permeable Artificial Water Channels That Can Self-Assemble into Two-Dimensional Arrays. *Proc. Natl. Acad. Sci. U.S.A.* **2015**, *112*, 9810−9815.
(49) Lang, C.; Ye, D.; Song, W.; Yao, C.; Tu, Y.-m.; Capparelli, C.; LaNasa, J. A.; Hickner, M. A.; Gomez, E. W.; Hickey, R. J.; Kumar, M. Biomimetic Separation of Transport and Matrix Functions in Lamellar Block Copolymer Channel-Based Membranes. *ACS Nano* **2019**, *13*, 8292−8302.
(50) Majumder, M.; Chopra, N.; Andrews, R.; Hinds, B. J. Enhanced Flow in Carbon Nanotubes. *Nature* **2005**, *438*, 44.
(51) Fornasiero, F.; Park, H. G.; Holt, J. K.; Stadermann, M.; Grigoropoulos, C. P.; Noy, A.; Bakajin, O. Ion Exclusion by Sub-2nm Carbon Nanotube Pores. *Proc. Natl. Acad. Sci. U.S.A.* **2008**, *105*, 17250−17255.
(52) Majumder, M.; Zhan, X.; Andrews, R.; Hinds, B. J. Voltage Gated Carbon Nanotube Membranes. *Langmuir* **2007**, *23*, 8624−8631.
(53) Hatakeyama, K.; Karim, M. R.; Ogata, C.; Tateishi, H.; Funatsu, A.; Taniguchi, T.; Koinuma, M.; Hayami, S.; Matsumoto, Y. Proton Conductivities of Graphene Oxide Nanosheets: Single, Multilayer, and Modified Nanosheets. *Angew. Chem., Int. Ed.* **2014**, *53*, 6997−7000.
(54) Sisson, A. L.; Shah, M. R.; Bhosale, S.; Matile, S. Synthetic Ion Channels and Pores (2004−2005). *Chem. Soc. Rev.* **2006**, *35*, 1269−1286.
(55) Song, W.; Kumar, M. Artificial Water Channels: Toward and beyond Desalination. *Curr. Opin. Chem. Eng.* **2019**, *25*, 9−17.
(56) Barboiu, M.; Gilles, A. From Natural to Bioassisted and Biomimetic Artificial Water Channel Systems. *Acc. Chem. Res.* **2013**, *46*, 2814−2823.
(57) Kang, Q.; Guo, W. Biomimetic Smart Nanopores and Nanochannels. In *Chemically Modified Nanopores and Nanochannels*; Elsevier Inc., 2017; pp 85−102.
(58) Mao, X.; Xu, M.; Wu, H.; He, X.; Shi, B.; Cao, L.; Yang, P.; Qiu, M.; Geng, H.; Jiang, Z. Supramolecular Calix[n]Arenes-Intercalated Graphene Oxide Membranes for Efficient Proton Conduction. *ACS Appl. Mater. Interfaces* **2019**, *11*, 42250−42260.
(59) Horner, A.; Pohl, P. Single-File Transport of Water through Membrane Channels. *Faraday Discuss.* **2018**, *209*, 9−33.
(60) Mann, D. J.; Halls, M. D. Water Alignment and Proton Conduction inside Carbon Nanotubes. *Phys. Rev. Lett.* **2003**, *90*, 195503.
(61) Köfinger, J.; Hummer, G.; Dellago, C. Macroscopically Ordered Water in Nanopores. *Proc. Natl. Acad. Sci. U.S.A.* **2008**, *105*, 13218−13222.
(62) Akeson, M.; Deamer, D. W. Proton Conductance by the Gramicidin Water Wire. Model for Proton Conductance in the F1F0 ATPases? *Biophys. J.* **1991**, *60*, 101−109.
(63) Ye, Y.; Gong, L.; Xiang, S.; Zhang, Z.; Chen, B. Metal−Organic Frameworks as a Versatile Platform for Proton Conductors. *Adv. Mater.* **2020**, *32*, 1907090.
(64) Geng, K.; He, T.; Liu, R.; Dalapati, S.; Tan, K. T.; Li, Z.; Tao, S.; Gong, Y.; Jiang, Q.; Jiang, D. Covalent Organic Frameworks: Design, Synthesis, and Functions. *Chem. Rev.* **2020**, *120*, 8814−8933.
(65) Budd, P. M.; McKeown, N. B.; Fritsch, D. Polymers of Intrinsic Microporosity (PIMs): High Free Volume Polymers for Membrane Applications. *Macromol. Symp.* **2006**, *245*−*246*, 403−405.
(66) Wang, Z.; Zhang, S.; Chen, Y.; Zhang, Z.; Ma, S. Covalent Organic Frameworks for Separation Applications. *Chem. Soc. Rev.* **2020**, *49*, 708−735.
(67) Chandra, S.; Kundu, T.; Dey, K.; Addicoat, M.; Heine, T.; Banerjee, R. Interplaying Intrinsic and Extrinsic Proton Conductivities in Covalent Organic Frameworks. *Chem. Mater.* **2016**, *28*, 1489−1494.
(68) Nagao, Y. Proton-Conductivity Enhancement in Polymer Thin Films. *Langmuir* **2017**, *33*, 12547−12558.
(69) Thomas, S. W., III; Joly, G. D.; Swager, T. M. Chemical Sensors Based on Amplifying Conjugated Polymers. *Chem. Rev.* **2007**, *107*, 1339−1386.
(70) Giuliani, M.; Morbioli, I.; Sansone, F.; Casnati, A. Moulding Calixarenes for Biomacromolecule Targeting. *Chem. Commun.* **2015**, *51*, 14140−14159.
(71) Yu, G.; Chen, X. Host−Guest Chemistry in Supramolecular Theranostics. *Theranostics* **2019**, *9*, 3041−3074.
(72) Webber, M. J. Dynamic Soft Materials as Tough Glass. *Nat. Mater.* **2022**, *21*, 6−7.
(73) Jie, K.; Zhou, Y.; Yao, Y.; Huang, F. Macrocyclic Amphiphiles. *Chem. Soc. Rev.* **2015**, *44*, 3568−3587.
(74) Addonizio, C. J.; Gates, B. D.; Webber, M. J. Supramolecular "Click Chemistry" for Targeting in the Body. *Bioconjugate Chem.* **2021**, *32*, 1935−1946.
(75) Markowitz, M. A.; Janout, V.; Castner, D. G.; Regen, S. L. Perforated Monolayers: Design and Synthesis of Porous and Cohesive Monolayers from Mercurated Calix[n]Arenes. *J. Am. Chem. Soc.* **1989**, *111*, 8192−8200.

https://doi.org/10.1021/jacsau.2c00143
JACS Au 2022, 2, 1144−1159

(76) Zhang, L.-h.; Hendel, R. A.; Cozzi, P. G.; Regen, S. L. A Single Langmuir−Blodgett Monolayer for Gas Separations. *J. Am. Chem. Soc.* **1999**, *121*, 1621−1622.
(77) Liang, Y.; Zhu, Y.; Liu, C.; Lee, K.-R.; Hung, W.-S.; Wang, Z.; Li, Y.; Elimelech, M.; Jin, J.; Lin, S. Polyamide Nanofiltration Membrane with Highly Uniform Sub-Nanometre Pores for Sub-1 Å Precision Separation. *Nat. Commun.* **2020**, *11*, 1−9.
(78) Elimelech, M.; Phillip, W. A. The Future of Seawater and the Environment. *Science* **2011**, *333*, 712−717.
(79) Faucher, S.; Aluru, N.; Bazant, M. Z.; Blankschtein, D.; Brozena, A. H.; Cumings, J.; Pedro De Souza, J.; Elimelech, M.; Epsztein, R.; Fourkas, J. T.; Rajan, A. G.; Kulik, H. J.; Levy, A.; Majumdar, A.; Martin, C.; McEldrew, M.; Misra, R. P.; Noy, A.; Pham, T. A.; Reed, M.; Schwegler, E.; Siwy, Z.; Wang, Y.; Strano, M. Critical Knowledge Gaps in Mass Transport through Single-Digit Nanopores: A Review and Perspective. *J. Phys. Chem. C* **2019**, *123*, 21309−21326.
(80) Epsztein, R.; DuChanois, R. M.; Ritt, C. L.; Noy, A.; Elimelech, M. Towards Single-Species Selectivity of Membranes with Sub-nanometre Pores. *Nat. Nanotechnol.* **2020**, *15*, 426−436.
(81) Choi, W.; Ulissi, Z. W.; Shimizu, S. F. E.; Bellisario, D. O.; Ellison, M. D.; Strano, M. S. Diameter-Dependent Ion Transport through the Interior of Isolated Single-Walled Carbon Nanotubes. *Nat. Commun.* **2013**, *4*, 2397.
(82) Zhou, X.; Heiranian, M.; Yang, M.; Epsztein, R.; Gong, K.; White, C. E.; Hu, S.; Kim, J.-H.; Elimelech, M. Selective Fluoride Transport in Subnanometer TiO2 Pores. *ACS Nano* **2021**, *15*, 16828−16838.
(83) Zheng, G.-L.; Yang, G.-C.; Song, S.-Y.; Song, X.-Z.; Zhang, H.-J. Constructing Porous MOF Based on the Assembly of Layer Framework and P-Sulfonatocalix[4]Arene Nanocapsule with Proton-Conductive Property. *CrystEngComm* **2014**, *16*, 64−68.
(84) Yang, W.; de Villiers, M. M. Effect of 4-Sulphonato-Calix[n]Arenes and Cyclodextrins on the Solubilization of Niclosamide, a Poorly Water Soluble Anthelmintic. *AAPS J.* **2005**, *7*, E241−E248.
(85) Eddaif, L.; Shaban, A.; Telegdi, J. Sensitive Detection of Heavy Metals Ions Based on the Calixarene Derivatives-Modified Piezoelectric Resonators: A Review. *Int. J. Environ. Anal. Chem.* **2019**, *99*, 824−853.
(86) Houmadi, S.; Coquière, D.; Legrand, L.; Fauré, M. C.; Goldmann, M.; Reinaud, O.; Rémita, S. Architecture-Controlled "SMART" Calix[6]Arene Self-Assemblies in Aqueous Solution. *Langmuir* **2007**, *23*, 4849−4855.
(87) Chen, M.-X.; Li, T.; Peng, S.; Tao, D. Supramolecular Nanocapsules from the Self-Assembly of Amphiphilic Calixarene as a Carrier for Paclitaxel. *New J. Chem.* **2016**, *40*, 9923−9929.
(88) Martin, A. D.; Raston, C. L. Multifunctional P-Phosphonated Calixarenes. *Chem. Commun.* **2011**, *47*, 9764−9772.
(89) Helttunen, K.; Shahgaldian, P. Self-Assembly of Amphiphilic Calixarenes and Resorcinarenes in Water. *New J. Chem.* **2010**, *34*, 2704−2714.
(90) Skorjanc, T.; Shetty, D.; Sharma, S. K.; Raya, J.; Traboulsi, H.; Han, D. S.; Lalla, J.; Newlon, R.; Jagannathan, R.; Kirmizialtin, S.; Olsen, J.-C.; Trabolsi, A. Redox-Responsive Covalent Organic Nanosheets from Viologens and Calix[4]Arene for Iodine and Toxic Dye Capture. *Chem.—Eur. J.* **2018**, *24*, 8648−8655.
(91) Abubakar, S.; Skorjanc, T.; Shetty, D.; Trabolsi, A. Porous Polycalix[n]Arenes as Environmental Pollutant Removers. *ACS Appl. Mater. Interfaces* **2021**, *13*, 14802−14815.
(92) Chung, H. T.; Cullen, D. A.; Higgins, D.; Sneed, B. T.; Holby, E. F.; More, K. L.; Zelenay, P. Direct Atomic-Level Insight into the Active Sites of a High-Performance PGM-Free ORR Catalyst. *Science* **2017**, *357*, 479−484.
(93) Wu, G.; More, K. L.; Johnston, C. M.; Zelenay, P. High-Performance Electrocatalysts for Oxygen Reduction Derived from Polyaniline, Iron, and Cobalt. *Science* **2011**, *332*, 443−447.
(94) DeCoursey, T. E. Voltage-Gated Proton Channels: Molecular Biology, Physiology, and Pathophysiology of the HV Family. *Physiol. Rev.* **2013**, *93*, 599−652.
(95) Robertson, K. M.; Tieleman, D. P. Molecular Basis of Voltage Gating of OmpF Porin. *Biochem. Cell Biol.* **2002**, *80*, 517−523.
(96) Litster, S.; Mclean, G. PEM Fuel Cell Electrodes. *J. Power Sources* **2004**, *130*, 61−76.
(97) Fuel Cell Multi-Year Research, Development, and Demonstration Plan. 2016, pp 1−58, https://www.energy.gov/sites/default/files/2017/05/f34/fcto_myrdd_fuel_cells.pdf (accessed March 1, 2022).
(98) Kumar, A.; Pisula, W.; Müllen, K. Effect of Humidity and Temperature on Proton Conduction in Phosphonated Copolymers. *Mater. Today Commun.* **2019**, *20*, 100539.
(99) Ahn, M.-K.; Lee, S.-B.; Min, C.-M.; Yu, Y.-G.; Jang, J.; Gim, M.-Y.; Lee, J.-S. Enhanced Proton Conductivity at Low Humidity of Proton Exchange Membranes with Triazole Moieties in the Side Chains. *J. Membr. Sci.* **2017**, *523*, 480−486.
(100) Wu, X.; Wang, X.; He, G.; Benziger, J. Differences in Water Sorption and Proton Conductivity between Nafion and SPEEK. *J. Polym. Sci., Part B: Polym. Phys.* **2011**, *49*, 1437−1445.
(101) Paul, D. K.; McCreery, R.; Karan, K. Proton Transport Property in Supported Nafion Nanothin Films by Electrochemical Impedance Spectroscopy. *J. Electrochem.* **2014**, *161*, F1395−F1402.
(102) Park, S.; Moilanen, D. E.; Fayer, M. D. Water Dynamics-The Effects of Ions and Nanoconfinement. *J. Phys. Chem. B* **2008**, *112*, 5279−5290.
(103) Ono, Y.; Nagao, Y. Interfacial Structure and Proton Conductivity of Nafion at the Pt-Deposited Surface. *Langmuir* **2016**, *32*, 352−358.
(104) Shrivastava, U. N.; Suetsugu, K.; Nagano, S.; Fritzsche, H.; Nagao, Y.; Karan, K. Cross-Correlated Humidity-Dependent Structural Evolution of Nafion Thin Films Confined on a Platinum Substrate. *Soft Matter* **2020**, *16*, 1190−1200.
(105) Gao, X.; Yamamoto, K.; Hirai, T.; Ohta, N.; Uchiyama, T.; Watanabe, T.; Takahashi, M.; Takao, N.; Imai, H.; Sugawara, S.; Shinohara, K.; Uchimoto, Y. Substrate-Dependent Proton Transport and Nanostructural Orientation of Perfluorosulfonic Acid Polymer Thin Films on Pt and Carbon Substrate. *Solid State Ionics* **2020**, *357*, 115456.
(106) Fayer, M. D. Dynamics of Water Interacting with Interfaces, Molecules, and Ions. *Acc. Chem. Res.* **2012**, *45*, 3−14.
(107) Hibbs, M. R.; Hickner, M. A.; Alam, T. M.; McIntyre, S. K.; Fujimoto, C. H.; Cornelius, C. J. Transport Properties of Hydroxide and Proton Conducting Membranes. *Chem. Mater.* **2008**, *20*, 2566−2573.
(108) Ohira, A.; Kuroda, S.; Mohamed, H. F. M.; Tavernier, B. Effect of Interface on Surface Morphology and Proton Conduction of Polymer Electrolyte Thin Films. *Phys. Chem. Chem. Phys.* **2013**, *15*, 11494−11500.
(109) Basilio, N.; Francisco, V.; Garcia-Rio, L. Aggregation of P-Sulfonatocalixarene-Based Amphiphiles and Supra-Amphiphiles. *Int. J. Mol. Sci.* **2013**, *14*, 3140−3157.
(110) Suwattanamala, A.; Magalhães, A. L.; Gomes, J. A. N. F. Computational Study of Calix[4]Arene Derivatives and Complexation with Zn2+. *Chem. Phys.* **2005**, *310*, 109−122.
(111) Park, M. J.; Balsara, N. P. Anisotropic Proton Conduction in Aligned Block Copolymer Electrolyte Membranes at Equilibrium with Humid Air. *Macromolecules* **2010**, *43*, 292−298.
(112) Avogadro: An Open-Source Molecular Builder and Visualization Tool. 2018, https://github.com/cryos/avogadro/ (accessed Nov. 5, 2021).
(113) Hanwell, M. D.; Curtis, D. E.; Lonie, D. C.; Vandermeersch, T.; Zurek, E.; Hutchison, G. R. Avogadro: An Advanced Semantic Chemical Editor, Visualization, and Analysis Platform. *J. Cheminf.* **2012**, *4*, 17.
(114) Aprà, E.; Bylaska, E. J.; De Jong, W. A.; Govind, N.; Kowalski, K.; Straatsma, T. P.; Valiev, M.; Van Dam, H. J. J.; Alexeev, Y.; Anchell, J.; Anisimov, V.; Aquino, F. W.; Atta-Fynn, R.; Autschbach,

https://doi.org/10.1021/jacsau.2c00143
JACS Au 2022, 2, 1144−1159

J.; Bauman, N. P.; Becca, J. C.; Bernholdt, D. E.; Bhaskaran-Nair, K.; Bogatko, S.; Borowski, P.; Boschen, J.; Brabec, J.; Bruner, A.; Cauët, E.; Chen, Y.; Chuev, G. N.; Cramer, C. J.; Daily, J.; Deegan, M. J. O.; Dunning, T. H.; Dupuis, M.; Dyall, K. G.; Fann, G. I.; Fischer, S. A.; Fonari, A.; Früchtl, H.; Gagliardi, L.; Garza, J.; Gawande, N.; Ghosh, S.; Glaesemann, K.; Götz, A. W.; Hammond, J.; Helms, V.; Hermes, E. D.; Hirao, K.; Hirata, S.; Jacquelin, M.; Jensen, L.; Johnson, B. G.; Jónsson, H.; Kendall, R. A.; Klemm, M.; Kobayashi, R.; Konkov, V.; Krishnamoorthy, S.; Krishnan, M.; Lin, Z.; Lins, R. D.; Littlefield, R. J.; Logsdail, A. J.; Lopata, K.; Ma, W.; Marenich, A. V.; Martin Del Campo, J.; Mejia-Rodriguez, D.; Moore, J. E.; Mullin, J. M.; Nakajima, T.; Nascimento, D. R.; Nichols, J. A.; Nichols, P. J.; Nieplocha, J.; Otero-De-La-Roza, A.; Palmer, B.; Panyala, A.; Pirojsirikul, T.; Peng, B.; Peverati, R.; Pittner, J.; Pollack, L.; Richard, R. M.; Sadayappan, P.; Schatz, G. C.; Shelton, W. A.; Silverstein, D. W.; Smith, D. M. A.; Soares, T. A.; Song, D.; Swart, M.; Taylor, H. L.; Thomas, G. S.; Tipparaju, V.; Truhlar, D. G.; Tsemekhman, K.; Van Voorhis, T.; Vázquez-Mayagoitia, Á.; Verma, P.; Villa, O.; Vishnu, A.; Vogiatzis, K. D.; Wang, D.; Weare, J. H.; Williamson, M. J.; Windus, T. L.; Woliński, K.; Wong, A. T.; Wu, Q.; Yang, C.; Yu, Q.; Zacharias, M.; Zhang, Z.; Zhao, Y.; Harrison, R. J. NWChem: Past, Present, and Future. *J. Chem. Phys.* **2020**, *152*, 184102.

(115) Spry, D. B.; Fayer, M. D. Proton Transfer and Proton Concentrations in Protonated Nafion Fuel Cell Membranes. *J. Phys. Chem. B* **2009**, *113*, 10210−10221.

(116) Fayer, M. D. Dynamics of Water Interacting with Interfaces, Molecules, and Ions. *Acc. Chem. Res.* **2012**, *45*, 3−14.

(117) Fayer, M. D.; Levinger, N. E. Analysis of Water in Confined Geometries and at Interfaces. *Annu. Rev. Anal. Chem.* **2010**, *3*, 89−107.

(118) Spry, D. B.; Goun, A.; Glusac, K.; Moilanen, D. E.; Fayer, M. D. Proton Transport and the Water Environment in Nafion Fuel Cell Membranes and AOT Reverse Micelles. *J. Am. Chem. Soc.* **2007**, *129*, 8122−8130.

(119) Baker, J. M.; Dore, J. C.; Seddon, J. M.; Soper, A. K. Structural Modification of Water in the Confined Layer of a Lamellar Lipid Crystal. *Chem. Phys. Lett.* **1996**, *256*, 649−652.

(120) Mondal, S. K.; Sahu, K.; Sen, P.; Roy, D.; Ghosh, S.; Bhattacharyya, K. Excited State Proton Transfer of Pyranine in a γ-Cyclodextrin Cavity. *Chem. Phys. Lett.* **2005**, *412*, 228−234.

(121) Gepshtein, R.; Leiderman, P.; Huppert, D.; Project, E.; Nachliel, E.; Gutman, M. Proton Antenna Effect of the γ-Cyclodextrin Outer Surface, Measured by Excited State Proton Transfer. *J. Phys. Chem. C* **2006**, *110*, 26354−26364.

(122) Mondal, S. K.; Sahu, K.; Ghosh, S.; Sen, P.; Bhattacharyya, K. Excited-State Proton Transfer from Pyranine to Acetate in γ -Cyclodextrin And Hydroxypropyl γ-Cyclodextrin. *J. Phys. Chem. A* **2006**, *110*, 13646−13652.

(123) Babu, S. K.; Chung, H. T.; Zelenay, P.; Litster, S. Resolving Electrode Morphology's Impact on Platinum Group Metal-Free Cathode Performance Using Nano-CT of 3D Hierarchical Pore and Ionomer Distribution. *ACS Appl. Mater. Interfaces* **2016**, *8*, 32764−32777.

(124) Li, Y.; Van Cleve, T.; Sun, R.; Gawas, R.; Wang, G.; Tang, M.; Elabd, Y. A.; Snyder, J.; Neyerlin, K. C. Modifying the Electrocatalyst − Ionomer Interface via Sulfonated Poly(Ionic Liquid) Block Copolymers to Enable High- Performance Polymer Electrolyte Fuel Cells. *ACS Energy Lett.* **2020**, *5*, 1726−1731.

(125) Avid, A.; Zenyuk, I. V. Confinement Effects for Nano-Electrocatalysts for Oxygen Reduction Reaction. *Curr. Opin. Electrochem.* **2021**, *25*, 100634.

(126) Li, D.; Lv, H.; Kang, Y.; Markovic, N. M.; Stamenkovic, V. R. Progress in the Development of Oxygen Reduction Reaction Catalysts for Low-Temperature Fuel Cells. *Annu. Rev. Chem. Biomol. Eng.* **2016**, *7*, 509−532.

(127) Lv, H.; Li, D.; Strmcnik, D.; Paulikas, A. P.; Markovic, N. M.; Stamenkovic, V. R. Recent Advances in the Design of Tailored Nanomaterials for Efficient Oxygen Reduction Reaction. *Nano Energy* **2016**, *29*, 149−165.

(128) Stamenkovic, V. R.; Fowler, B.; Mun, B. S.; Wang, G.; Ross, P. N.; Lucas, C. A.; Markovic, N. M. Improved Oxygen Reduction Activity on Pt3Ni(111) via Increased Surface Site Availability. *Science* **2007**, *315*, 493−497.

https://doi.org/10.1021/jacsau.2c00143
JACS Au 2022, 2, 1144−1159